Analysis of NMR spin-lattice relaxation rates in cuprates

A. Uldry and P. F. Meier
Physics Institute, University of Zurich, CH-8057 Zurich, Switzerland
(Received 2 February 2005; revised manuscript received 5 July 2005; published 16 September 2005)

We investigate nuclear spin-lattice relaxation data in the normal state of optimally doped $YBa_2Cu_3O_7$ by analyzing the contributions to the relaxation rate of the copper, planar oxygen, and yttrium along the directions perpendicular to the applied field. In this picture, there is no contrasting temperature dependence of the copper and oxygen relaxation. We use the model of fluctuating fields to express the rates in terms of hyperfine interaction energies and an effective correlation time τ_{eff} characterizing the dynamics of the spin fluid. The former contain the effects of the antiferromagnetic static spin correlations, which cause the hyperfine field constants to be added coherently at low temperature and incoherently at high temperature. The degree of coherency is therefore controlled by the spin-spin correlations. The model is used to determine the temperature-dependent correlation lengths. The temperature-dependent effective correlation time is found to be made up of a linear and a constant contribution that can be related to scattering and spin fluctuations of localized moments, respectively. The extrapolation of our calculation at higher temperature also fits the data very well at those temperatures. The underdoped compounds $YBa_2Cu_3O_{6.63}$ and $YBa_2Cu_4O_8$ are studied in the limit of the data available with some success by modifying the effective correlation time with a gap parameter. The copper data of the $La_{2-x}Sr_xCuO_4$ series are then discussed in terms of the interplay between the two contributions to τ_{eff}.

DOI: 10.1103/PhysRevB.72.094508 PACS number(s): 74.25.−q, 74.25.Ha, 76.60.−k

I. INTRODUCTION

The nuclear resonance techniques, nuclear magnetic resonance (NMR), and nuclear quadrupole resonance (NQR), are powerful probes for investigating the microscopic magnetic properties of cuprates that exhibit high-temperature superconductivity. An important advantage of these methods is based on their highly local nature, which allows one to get information about the distinct chemical species in the materials and make selective measurements of different crystallographic sites (for reviews, see Refs. 1–4). Magnetic hyperfine interactions couple the nuclear spins to the electron system, and it is essential that they are determined as accurately as possible in order to allow a correct interpretation of the properties of the electron liquid in terms of measured NMR or NQR data.

One particular aspect that has absorbed the attention of the NMR community is that the experiments in $YBa_2Cu_3O_7$, $YBa_2Cu_3O_{6.63}$, and $La_{1.85}Sr_{0.15}CuO_4$ (Refs. 5–13) seem to show a dramatic contrast in nuclear spin-lattice relaxation rate behavior between copper and oxygen sites in the CuO_2 plane, although these sites lie less than 2 Å apart. It was concluded that the relaxation at the copper site exhibits strong antiferromagnetic (AFM) enhancement effects, whereas that at the planar oxygen site is weakly enhanced with strikingly different temperature dependence.

The nuclear spin-lattice relaxation rate ${}^kT_{1\alpha}^{-1}$ for a nuclear species k is the rate at which the magnetization relaxes to its equilibrium value in the external magnetic field applied in direction α. The relaxation of the nuclei under consideration in the cuprates is caused by two or more fluctuating hyperfine fields that originate from magnetic moments localized near the coppers. Since the squares of these fields come into play, one of the first tasks when interpreting spin-lattice relaxation data is to determine whether the hyperfine fields should be added coherently or incoherently at the nucleus. While Mila and Rice[14] added them incoherently, Monien, Pines, and Slichter[15] considered both extreme cases and, from the analysis of the copper data in $YBa_2Cu_3O_7$, concluded that within a one-component model, the fields should be added coherently. The question of coherency was put aside when Millis, Monien, and Pines (MMP) gave a quantitative and complete phenomenological description of the relevant measurements by putting forward a model[16] in which the nuclear spin-lattice relaxation rate, via the fluctuation-dissipation theorem, is expressed in terms of the low-frequency limit of the imaginary part of the spin susceptibility χ

$$ {}^kT_{1\alpha}^{-1} \propto \sum_q {}^kF_\alpha(\vec{q}) \lim_{\omega\to 0}(\chi''(\vec{q},\omega)/\omega). \tag{1}$$

The form factors ${}^kF_\alpha(\vec{q})$ depend on the geometrical arrangements of the nuclei and the localized electronic spins. Under the form Eq. (1), the question of the degree of coherency is delegated to the choice of a form for the susceptibility. The basic idea behind the MMP model was to account for strong AFM correlations, which exist in the cuprates even in the overdoped regime. The MMP model therefore postulated a spin susceptibility that is strongly peaked at the AFM wave vector $\vec{Q}=(\pi,\pi)$. In this way, the seemingly different relaxation behavior of copper and oxygen could be understood, and almost all NMR and NQR relaxation measurements in cuprates have been analyzed using the MMP approach. In a later development of the model,[17] the susceptibility $\chi(q,\omega)$ was split into two parts, $\chi=\chi_{AF}+\chi_{FL}$. The first term, χ_{AF}, represents the anomalous contribution to the spin system and is peaked at or near $\vec{Q}$. The second term, χ_{FL}, is a param-

etrized form of the normal Fermi-liquid contribution. For copper, the contributions from the Fermi-liquid part are much smaller than those from χ_{AF}, but they dominate the relaxation of oxygen and yttrium nuclei. In the parametrization for χ introduced by MMP, χ_{AF} is strongly peaked at $\vec{Q}$, and the hyperfine fields at the copper are added essentially coherently. On the other hand, for any $\vec{q}$-independent χ_{FL}, the contributions of these fields are strictly incoherent, and the fields at the oxygen are therefore added incoherently in the MMP theory.

The goal of our work is to get the information about the degree of coherency directly from the data. We therefore intentionally avoid the use of Eq. (1), since the degree of coherency of the hyperfine fields at a nucleus depends on details of the susceptibility, which are difficult to model. Moreover, the possibility that two or more processes contribute to the spin relaxation might make it difficult to disentangle these different contributions. We therefore stay in the direct space, since there are only a few points in the lattice that are relevant for NMR. In this case, the coherency is related to the spin-spin correlations, which we take as a parameter that we deduce from the experiments. The spin-spin correlations are found to be temperature dependent, and therefore, the degree of coherency varies with the temperature. As expected, the coherency is reduced when the temperature is increased. We note that this is also what MMP finds in the case of the copper nuclei—the peak in the susceptibility (as well as the sometimes forgotten cutoff[16]) gets broader as the correlations decrease. However, the approach taken here reveals other advantages—in contrast to MMP, the relaxation of both the copper and the oxygen (as well as the yttrium) is caused by the *same* temperature-dependent relaxation mechanism of the spin liquid, which we will characterize by an effective correlation time. Also, the different temperature behavior of the oxygen and the copper nuclear relaxation rates can then be explained naturally from the particular values of the hyperfine field constants.

The premises of our different approach to the analysis of spin-lattice relaxation data in the normal state of cuprates are the following: (i) We go back to the simple model of fluctuating fields[18] that has been applied by Pennington *et al.*[19] to analyze their spin-lattice relaxation rate data for copper in $YBa_2Cu_3O_7$. This model is particularly appropriate for anisotropic substances, as it is the case of the cuprates. We retain, however, the AFM correlations, which are an essential feature of the concept of the nearly AFM Fermi liquid. The normalized AFM spin-spin correlations between adjacent coppers are a key quantity, since they determine to what extent the hyperfine fields are added coherently. (ii) We adopt the usual form for the spin Hamiltonian for copper as proposed by Mila and Rice,[14] whereas that for the oxygen is determined by transferred contributions from the two nearest neighbor copper ions (Shastry[20]). We note that quantum-chemical calculations[21,22] have shown that contributions to the oxygen hyperfine interaction arising from farther-distant copper ions are marginal and that an introduction of a substantial transferred field from the next-nearest-neighbor Cu is not justified. (iii) We will assume that all data obtained in the normal state of the cuprates can be attributed to purely magnetic relaxation, although there are indications[23] that some observed phenomena hint at an additional influence of charge fluctuations. (iv) We confine our analysis to measurements of the planar copper and oxygen and the yttrium nuclei in the normal state. We neglect orthorhombicity and assume a quadratic CuO_2 plane with a lattice constant of unity. For the planar oxygen, we distinguish between the direction *a*, par-

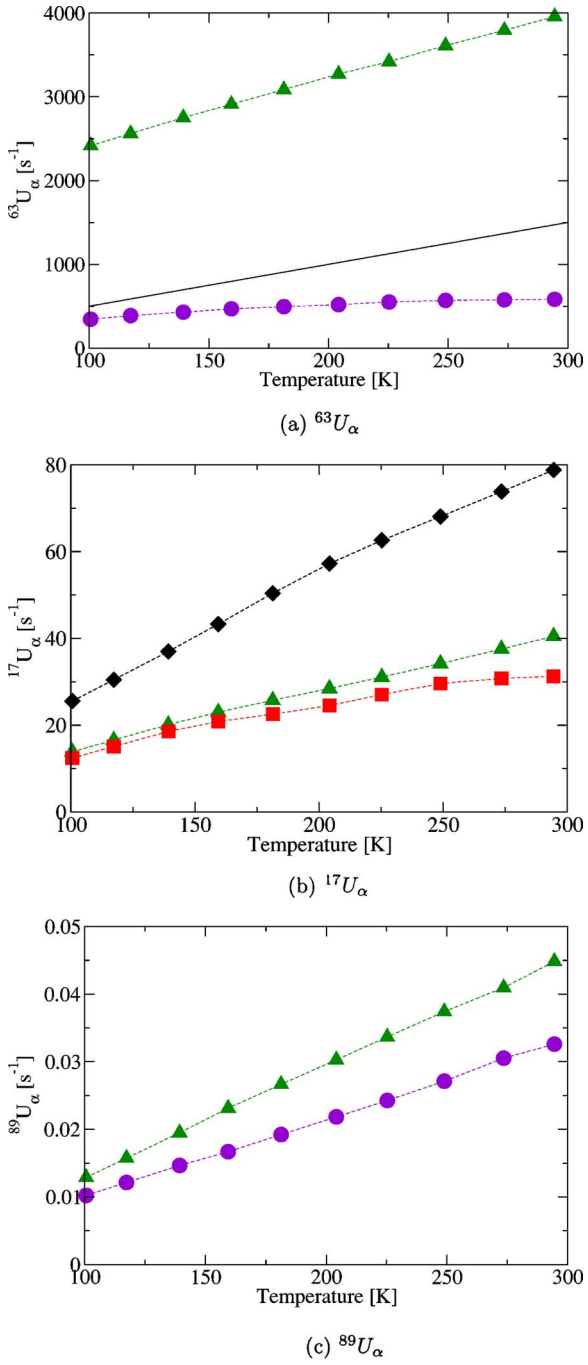

FIG. 1. (Color online) Relaxation rates $^kU_\alpha$ from measurements in $YBa_2Cu_3O_7$. The symbols denote interpolations of $T_{1\alpha}^{-1}$ data (Refs. 8 and 25–27) transformed according to Eq. (3), in the direction *a* (diamonds), *b* (squares), *ab* (circles), and *c* (triangles). Dashed lines are for readability. The solid straight line in (a) denotes the values for metallic copper.

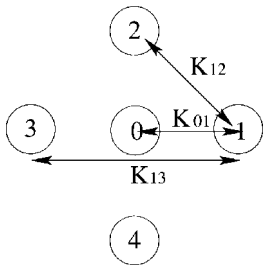

FIG. 2. Schematic diagram of the AFM spin correlations K_{ij} between electron moments at the copper sites 0,1,…,4.

allel to the Cu-O-Cu bond, and b, perpendicular to the bond.

Our work is structured as follows: We introduce in Sec. II a representation of the relaxation data that is appropriate to their analysis in anisotropic materials. Section III presents the model and the assumptions made. We then apply our treatment to $YBa_2Cu_3O_7$ in Sec. IV and test our results with a range of experiments, in particular, those made at high temperature. The significance of the model parameters at low temperature are discussed. Due to lack of data, the underdoped materials $YBa_2Cu_3O_{6.63}$ and $YBa_2Cu_4O_8$ are less extensively treated in Sec. V. We turn to the $La_{2-x}Sr_xCuO_4$ series in Sec. VI and discuss the temperature and doping dependence in view of our model, in particular, in the high-temperature limit. We present a summary and conclusions in Sec. VII. Some special considerations are collected in the Appendixes.

II. REPRESENTATION OF DATA FOR ANISOTROPIC MATERIALS

In this section, we plot the spin-lattice relaxation data in a way that suggests that the same relaxation mechanism is at work for all the nuclei under consideration. The magnetic relaxation process into equilibrium is caused by fluctuating effective magnetic fields along the two orthogonal axes β and γ perpendicular to the direction α of the applied field, which we write as

$$^kT_{1\alpha}^{-1} = {}^kU_\beta + {}^kU_\gamma, \tag{2}$$

where $(\alpha,\beta,\gamma)=(x,y,z)$. The quantities $^kU_\alpha$ describe the contribution to $^kT_{1\beta}^{-1}$ and $^kT_{1\gamma}^{-1}$ caused by fluctuating fields in the crystallographic direction α. From Eq. (2), the $^kU_\alpha$ are therefore given by

$$^kU_\alpha = \frac{1}{2}(-{}^kT_{1\alpha}^{-1} + {}^kT_{1\beta}^{-1} + {}^kT_{1\gamma}^{-1}). \tag{3}$$

These transformed rates $^kU_\alpha$, which in the following will just be called rates, are not directly accessible by experiment except for particular symmetries (e.g., $^{63}U_{ab}={}^{63}T_{1c}^{-1}/2$), but in general can be obtained if a complete set of data measured with the applied field along all three crystallographic axes is available. At variance with the common representation of NMR spin-lattice relaxation rates in $(T_1T)^{-1}$ vs T plots, we prefer here to study the rates U_α. This change in representation is trivial. It was, however, pointed out earlier by one of us[24] that it is much more instructive to investigate ratios between $^kU_\alpha$ for α in different directions than ratios of the corresponding rates $^kT_{1\alpha}^{-1}$.

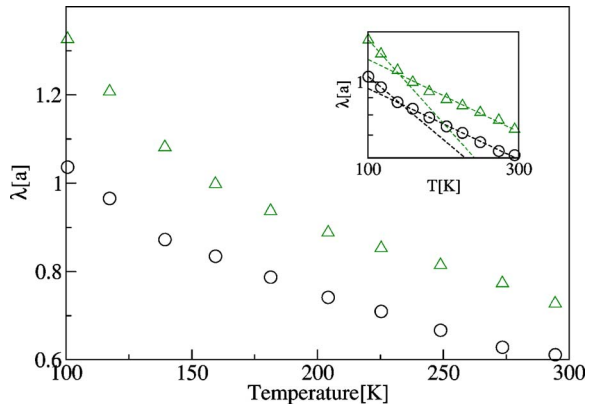

FIG. 3. (Color online) Correlation lengths λ_α obtained from the fit in $YBa_2Cu_3O_7$, in the direction ab (circles) and c (triangles). Inset: the same on a logarithmic scale, fitted with exponential functions.

The practice of representing and analyzing $(T_1T)^{-1}$ data grew from applications in liquids where the rates are isotropic and $(T_1T)^{-1}$ is temperature independent in simple metals. For layered cuprates, however, which are anisotropic materials, the analysis of NMR data in terms of $^kU_\alpha$ has distinct advantages over that in terms of $^kT_{1\alpha}^{-1}$.

For cuprates, the most complete set of NMR and NQR data with respect to different nuclei and directions of external field relative to the crystallographic axes is available for optimally doped $YBa_2Cu_3O_7$ in the normal state between 100 K and room temperature. We start our analysis, therefore, in this temperature range and use the copper data for $^{63}T_{1c}^{-1}$ from Hammel *et al.*[8] and $^{63}T_{1ab}^{-1}$ from Walstedt *et al.*[25] The oxygen data $^{17}T_{1\alpha}^{-1}$ were taken from Martindale *et al.*,[26] and the yttrium data $^{89}T_{1\gamma}^{-1}$ from Takigawa *et al.*[27]

These sets of data for the rates $^kT_{1\alpha}^{-1}$, interpolated at the same temperature points, allow the transformation into our rates $^kU_\alpha$ according to Eq. (3). Neglecting any error analysis, the results for the three nuclei are shown in Fig. 1.

In these representations of the data, there is no sign of a drastic contrast in the temperature dependence of the relaxation rates of copper and oxygen nuclei in the same CuO_2 plane that has, as mentioned in the Introduction, intrigued the NMR community. All relaxation rates grow with increasing temperature, as is expected for fluctuations. The differences in the magnitude for Cu, O, and Y are due to different strengths of the hyperfine interaction energies, which allow a scaling of all data, as is shown in Appendix A. We stress that so far no model is used, and nothing else was done other than adding and subtracting the data.

The relaxation rate data, transformed now into a representation appropriate for layered structures, suggest therefore that all nuclei under consideration relax in a *similar* fashion by the same mechanism of the spin liquid and that the strength of this relaxation initially increases linearly with temperature. [Note that the additional line drawn in Fig. 1(a) depicts the relaxation measured in copper metal.] The question of why the relaxation rates between the copper and the

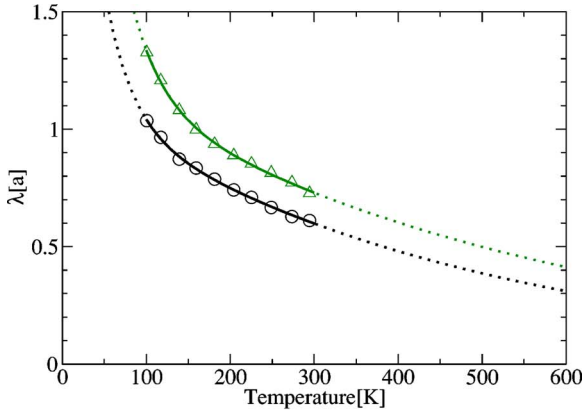

(a) Correlation lengths λ_α

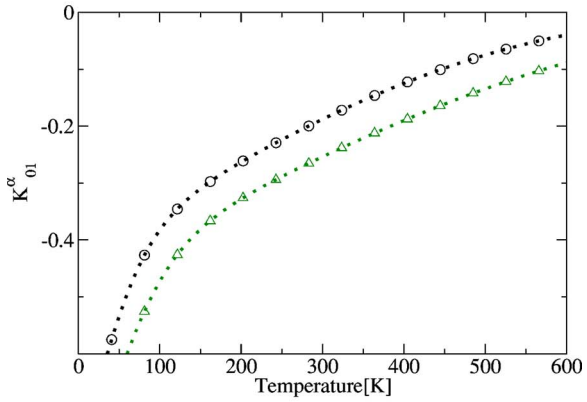

(b) NN AFM spin correlations K^α_{01}

FIG. 4. (Color online) Correlations and correlation lengths from the fit (lines) in the direction *ab* (circles) and *c* (triangles). The dotted lines are extrapolations with exponential functions.

oxygen are nonetheless *different* will be investigated in Sec. IV F. In the following section, we outline a robust and unbiased model that will allow us to deduce more details about the origin and the source of the temperature dependence of the spin-lattice relaxation.

III. MODEL AND ASSUMPTIONS

The quantities ${}^kU_\alpha$ have been introduced as the contributions from fluctuating local effective magnetic fields H_α along the direction α. In this section, we adopt the calculation of relaxation rates in terms of fluctuating fields described in Ref. 18 to determine an expression for ${}^kU_\alpha$ in the present case. In particular, in the cuprates, the hyperfine interaction energies depend on the static AFM spin correlations. We find that ${}^kU_\alpha$, for any nuclei k under consideration, can be written as a static term containing the spin correlations and hyperfine field constants and another term that is the effective correlation time.

Let us consider first an oxygen nucleus with spin ${}^{17}I$ and gyromagnetic ratio ${}^{17}\gamma$, for which the hyperfine interaction Hamiltonian is determined by

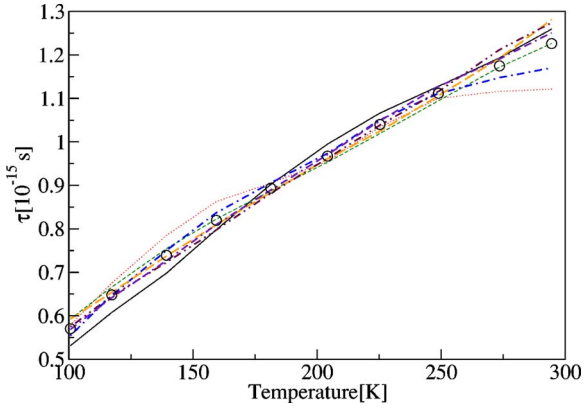

FIG. 5. (Color online) Relaxation times obtained from the experimental rates ${}^kU_\alpha$ using the fitted correlations and hyperfine fields. The circles are the calculated average; ${}^{17}\tau_a$ (thin solid line), ${}^{17}\tau_b$ (thin dotted line), ${}^{17}\tau_c$ (thin dashed line), ${}^{63}\tau_{ab}$ (thick dashed-dotted line), ${}^{63}\tau_c$ (thick dashed line), ${}^{89}\tau_{ab}$ (thick dash-dot-dot-dashed line), and ${}^{89}\tau_c$ (thick dot-dash-dash-dotted line).

$$ {}^{17}\mathcal{H}(t) = -\hbar\,{}^{17}\gamma\,{}^{17}\vec{H}(t)\cdot{}^{17}\vec{I}. \tag{4}$$

The field operator ${}^{17}\vec{H}(t)$ for an oxygen situated between sites 0 and 1 (Fig. 2) is assumed to originate from magnetic moments with spin $S=\frac{1}{2}$ localized on those two adjacent nearest-neighbor (NN) copper ions with spin components S^0_α and S^1_α, respectively. The field operator components are given by

$$ {}^{17}H_\alpha(t) = -\hbar\,\gamma_e c_\alpha [S^0_\alpha(t) + S^1_\alpha(t)], \tag{5}$$

where c_α is the diagonal element of the hyperfine tensor in direction α given in units of spin densities (a_B^{-3}).

Provided that the fluctuations in different field directions are independent, the components of the autocorrelation function of ${}^{17}H(t)$ are

$$ \langle {}^{17}H_\alpha(t)\,{}^{17}H_\alpha(0)\rangle = \hbar^2\gamma_e^2 c_\alpha^2 2\langle S^\alpha_0(t)S^\alpha_0(0) + S^\alpha_0(t)S^\alpha_1(0)\rangle. \tag{6}$$

Assuming an exponential decay of correlations in time, the expression in brackets can be written as

$$ \langle S^\alpha_0(t)S^\alpha_0(0) + S^\alpha_0(t)S^\alpha_1(0)\rangle = \frac{1}{4}(1+K^\alpha_{01})e^{-|t|/\tau_{eff}}. \tag{7}$$

τ_{eff} is an effective correlation time that acts as a time scale for the fluctuations.[18] Its temperature dependence will give us an indication as to what type of processes come into play in the relaxation. K^α_{01} is the normalized "static" NN spin correlation

$$ K^\alpha_{01} = 4\langle S^\alpha_0(0)S^\alpha_1(0)\rangle. \tag{8}$$

The correlations of two NN moments is thus separated into a spatial AFM correlation K^α_{01} that will determine the degree of coherency and temporal correlation that characterizes the dynamics of the electronic spin fluid system that exchanges energy with the nuclei.

We make the assumption that the correlation time τ_{eff} is isotropic and, in the following, that it is also independent of the spatial separation of the correlated spins. However, K_{01}^{α} may be different for in-plane and out-of-plane components. Following Slichter,[18] we find that ${}^{k}U_{\alpha}$ is obtained as

$$ {}^{k}U_{\alpha} = \frac{1}{2\hbar^2}\int_{-\infty}^{\infty} \langle {}^{k}H_{\alpha}(t)\,{}^{k}H_{\alpha}(0)\rangle e^{i\omega_k t}dt, \tag{9} $$

where ω_k is the Larmor frequency. The expression for the contribution ${}^{17}U_{\alpha}$ to the relaxation rate then is given by

$$ {}^{17}U_{\alpha} = \frac{2C_{\alpha}^2}{4\hbar^2}(1+K_{01}^{\alpha})\tau_{eff}, \tag{10} $$

when $|\omega_k \tau_{eff}| \ll 1$, with $C_{\alpha} = \hbar\,{}^{17}\gamma\hbar\,\gamma_e c_{\alpha}$.

The hyperfine field at the planar copper nucleus is determined by an on-site contribution A_{α} from the copper ion with spin component S_0^{α} and transferred contributions B_{α} from the four NN ions with spin components S_j^{α}, where $j=1,2,3,4$ (Fig. 2). We note that *ab initio* calculations of the hyperfine interactions[21,22] yield, in addition to the isotropic transferred field B, also a transferred dipolar field $B_{dip,\alpha}$, which, for simplicity, will be ignored in the following. The corresponding equation for ${}^{63}U_{\alpha}$ then reads

$$ {}^{63}U_{\alpha} = \frac{1}{4\hbar^2}(A_{\alpha}^2 + 4B^2 + 8A_{\alpha}BK_{01}^{\alpha} + 8B^2K_{12}^{\alpha} + 4B^2K_{13}^{\alpha})\tau_{eff}, \tag{11} $$

where K_{12}^{α} and K_{13}^{α} are the normalized spin correlations between two copper ions that are $\sqrt{2}$ and 2 lattice units apart, respectively (Fig. 2).

In the YBaCuO compounds, the yttrium is located between two adjacent CuO_2 planes and has four copper NN in each. Here, the situation is not as clear as for the Cu and O hyperfine interactions, since there may be interplane spin correlations between copper moments and a direct dipolar coupling of the same order magnitude as the transferred fields. We ignore these complications and use the simplest form, which leads to

$$ {}^{89}U_{\alpha} = \frac{8D_{\alpha}^2}{4\hbar^2}(1+2K_{01}^{\alpha}+K_{12}^{\alpha})\tau_{eff}. \tag{12} $$

It is convenient to express the relaxation rates as

$$ {}^{k}U_{\alpha}(T) = {}^{k}V_{\alpha}(T)\,\tau_{eff}(T), \tag{13} $$

with

$$ {}^{17}V_{\alpha}(T) = \frac{1}{4\hbar^2}2C_{\alpha}^2[1+K_{01}^{\alpha}(T)], \tag{14a} $$

$$ {}^{63}V_{\alpha}(T) = \frac{1}{4\hbar^2}[A_{\alpha}^2 + 4B^2 + 8A_{\alpha}BK_{01}^{\alpha}(T) + 8B^2K_{12}^{\alpha}(T) + 4B^2K_{13}^{\alpha}(T)], \tag{14b} $$

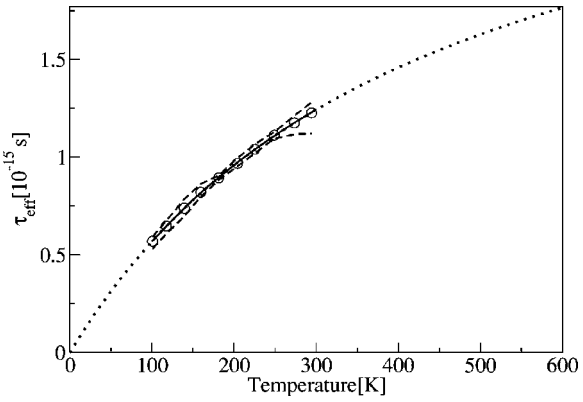

FIG. 6. Temperature dependence of the averaged relaxation time τ_{eff}. The circles are the calculated average, and the dashed lines represent the upper and lower bounds. The dotted line is the fit as explained in the text.

$$ {}^{89}V_{\alpha}(T) = \frac{1}{4\hbar^2}8D_{\alpha}^2[1+2K_{01}^{\alpha}(T)+K_{12}^{\alpha}(T)]. \tag{14c} $$

This factorization emphasizes the different temperature dependencies that determine ${}^{k}U_{\alpha}(T)$. The ${}^{k}V_{\alpha}(T)$, which, apart from the factor $\hbar^2$, are the static hyperfine energies squared, vary with temperature due to changes of the static spin correlations $K_{ij}^{\alpha}(T)$, whereas the effective correlation time $\tau_{eff}(T)$ reflects the changes in the dynamics.

We denote the limiting values when all correlations are zero by ${}^{k}V_{\alpha}^{0}$

$$ {}^{63}V_{\alpha}^{0} = \frac{1}{4\hbar^2}(A_{\alpha}^2 + 4B^2), \tag{15a} $$

$$ {}^{17}V_{\alpha}^{0} = \frac{1}{4\hbar^2}2C_{\alpha}^2, \tag{15b} $$

$$ {}^{89}V_{\alpha}^{0} = \frac{1}{4\hbar^2}8D_{\alpha}^2, \tag{15c} $$

and by ${}^{k}V_{\alpha}^{fc}$ for full AFM correlations

$$ {}^{63}V_{\alpha}^{fc} = \frac{1}{4\hbar^2}(A_{\alpha}-4B)^2, \tag{16a} $$

$$ {}^{17}V_{\alpha}^{fc} = 0, \tag{16b} $$

$$ {}^{89}V_{\alpha}^{fc} = 0. \tag{16c} $$

${}^{k}V_{\alpha}(T)$ accounts for the transition from the fully correlated situation, where the hyperfine fields are added coherently, toward the completely uncorrelated regime given by ${}^{k}V_{\alpha}^{0}$, where the fields are added incoherently.

We would like to point out that the model we use is an extension of a well-established approach. It has been applied, e.g., by Monien, Pines, and Slichter[15] to analyze ${}^{63}T_1^{-1}$ data in the limiting cases ${}^{63}V^{0}$ and ${}^{63}V^{fc}$. Here, we investigate the crossover between these limits by including the existence of AFM correlations in the cuprates that are static with respect

TABLE I. Magnetic hyperfine interaction energies in units of 10^{-6} eV.

	$^{63}A_c$	$^{63}A_{ab}$	^{63}B	$^{63}B_{dip,c}$	$^{17}C_a$	$^{17}C_b$	$^{17}C_c$	$^{89}D_{ab}$	$^{89}D_c$
Fit	−1.68	0.168	0.438	-	0.259	0.173	0.196	−0.00280	−0.00349
Reference 29	−1.6	0.29	0.4	-	0.25	0.13	0.156	−0.0048	−0.0048
Reference 22[a]	−1.72±0.42	0.21±0.11	0.29	0.05	0.289	0.140	0.151	-	-

[a]Cluster calculations. The error intervals are due to uncertainties in the spin-orbit interaction.

to typical NMR times and vary with the temperature.

In order to reduce the number of parameters, we assume that the static spin correlations are antiferromagnetic and that K_{12}^{α} and K_{13}^{α} depend directly on the value of K_{01}^{α}, according to

$$K_{12}^{\alpha} = |K_{01}^{\alpha}|^{\sqrt{2}} \quad \text{and} \quad K_{13}^{\alpha} = |K_{01}^{\alpha}|^2. \tag{17}$$

This particular choice of an exponential decay with length λ_α, defined so that

$$K_{01}^{\alpha} = -\exp(-1/\lambda_\alpha), \tag{18}$$

is guided by results of solutions of the planar anisotropic Heisenberg model, which were obtained by direct diagonalization of the Hamiltonian for small systems[28] and which suggested $K_{12}^{\alpha} \approx |K_{01}^{\alpha}|^{1.5}$ and anisotropic correlations.

These assumptions certainly influence the actual values for λ_α that will result from the analysis of the data, but they provide a reasonable starting point for the analysis and may be easily modified.

IV. RESULTS FOR $YBa_2Cu_3O_7$

We present in this section the analysis of the optimally doped $YBa_2Cu_3O_7$ data in the framework of our model. We first outline the fitting procedure, which allows us to determine the correlation lengths λ_{ab} and λ_c, and the hyperfine field constants. We can then determine the effective correlation time τ_{eff} and parametrize it in order to identify the underlying mechanisms of the spin fluid. We discuss in particular the low-temperature limit, which exhibits a Fermi-liquid character for all three nuclei (Cu, O, and Y). The model predictions at high temperature are then compared with experiments. Then, by looking at the extremal values of $^kV_\alpha$, we will discuss why the measured relaxation rates of the copper and oxygen have different temperature dependence. Finally, we apply our model to spin-spin relaxation measurements.

A. Fitting procedures

We define the following independent ratios r_j:

$$r_1 = \frac{^{63}U_c}{^{17}U_c}, \quad r_2 = \frac{^{63}U_{ab}}{^{17}U_a}, \quad r_3 = \frac{^{63}U_{ab}}{^{17}U_b}, \quad r_4 = \frac{^{17}U_b}{^{17}U_c},$$
$$r_5 = \frac{^{89}U_c}{^{89}U_{ab}}, \quad r_6 = \frac{^{17}U_c}{^{89}U_c}, \tag{19}$$

and denote with r_j^{exp} the ratios obtained from the experimental values for $^kU_\alpha$ as calculated from (3) and plotted in Fig. 1. We also form the ratios r_j^{mod} according to the model [Eqs. (10)–(12)], for which the correlation times τ_{eff} cancel ($r_1^{mod} = {}^{63}V_c/{}^{17}V_c$, etc.).

We define the following function to minimize:

$$\chi^2 = \frac{1}{n_r}\sum_i^{n_r}\sum_j^{n_p}\left(\frac{r_i^{exp}(T_j) - r_i^{mod}(T_j)}{r_i^{exp}(T_j)}\right)^2, \tag{20}$$

where n_r (6, in the case of $YBa_2Cu_3O_7$) is the number of ratios available, and j runs through the temperature points. The function measures the normalized difference between the calculated ratios r_i^{mod} and the experimental points r_i^{exp} at each temperature. We then minimize (20) in order to obtain the best local solution for the whole set of parameters (hyperfine interaction energies and values for the correlation lengths). As input parameters for the hyperfine interaction energies, we used the values determined by Höchner.[28] The λ_{ab} and λ_c obtained for each temperature point are illustrated in Fig. 3, and the resulting values for the hyperfine interaction energies[48] are given in Table I. It is seen in Fig. 3 that λ_c is consistently somewhat larger than λ_{ab} ($\lambda_c \approx 1.2\lambda_{ab}$), which could be related to our neglect of anisotropies in the g factors. From the logarithmic representation in the inset of Fig. 3, we see that the temperature dependence obtained for the λ_α can be parametrized by a sum of two exponential functions. This parametrization has been used only to extrapolate at higher and lower temperatures [dotted lines in Fig. 4(a)]. We would like to emphasize that we are not at this stage looking into interpreting the temperature dependence of λ_α. We merely want the λ_α to be optimally fitted (regardless of the significance of the parameters), and this particularly at high temperature.

The NN spin correlation functions K_{01}^{α} are plotted in Fig. 4(b). The correlation K_{01}^{ab} is about −0.4 at $T=100$ K and drops to −0.2 at room temperature. The extrapolation to higher temperatures shows that even at $T=600$ K, small AFM correlations (≈ -0.04) exist. It is clear that these specific values depend on the particular choice [Eq. (17)] of exponential dependence of the correlations with the distance.

We note that the hyperfine interaction energies in Table I have been determined only from relaxation data, without recourse to static measurements except that some reasonable initial guess had to be assumed. It is surprising that the re-

TABLE II. $^kV_\alpha^0$ in units of 10^{15} s^{-2}.

$^{17}V_a^0$	$^{17}V_b^0$	$^{17}V_c^0$	$^{63}V_{ab}^0$	$^{63}V_c^0$	$^{89}V_{ab}^0$	$^{89}V_c^0$
77.7	34.6	44.2	459.0	2080.0	0.0361	0.0562

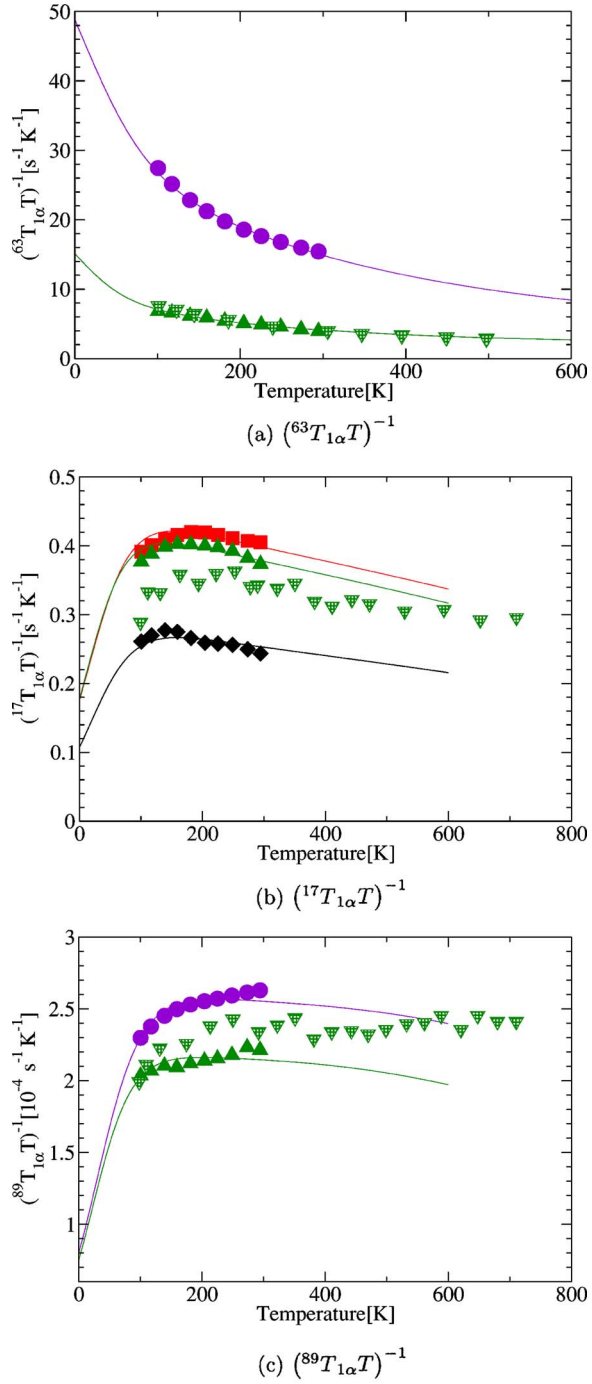

FIG. 7. (Color online) Full symbols denote the original experimental data. Lines denote the fit as explained in the text. Hashed symbols denote the other data (see text), with directions *a* (diamonds), *b* (squares), *ab* (circles), and *c* (triangles).

sulting values are very close to those that have been compiled by Nandor *et al.*[29] and that are included in Table I.

For further reference, we collect in Table II the values obtained for ${}^{k}V_{\alpha}^{0}$ calculated from (15) using the hyperfine interaction energies given in Table I.

B. Consistency check

In the preceding subsection, we formed the ratios r_i^{mod} in order to get rid of the effective correlation time τ_{eff} in the model. Having now the fitted values for the hyperfine interaction parameters and for $K_{01}^{\alpha}(T)$ and thus calculated the values ${}^{k}V_{\alpha}$ [Eq. (14)], we get back to the experimental spin-lattice relaxation rates ${}^{k}U_{\alpha}$. From (13), we can obtain the resulting seven experimental values ${}^{k}\tau_{eff,\alpha}$, which, according to the model assumptions, should all be equal. These seven values for τ_{eff} are plotted in Fig. 5 as a function of the temperature. The consistency is surprisingly good. We therefore calculated the mean values (circles in Fig. 5, neglecting any weighting according to the estimated precision of the data for the various nuclei).

The temperature dependence of the average τ_{eff} is well fit by a function in the form

$$\tau_{eff}^{-1} = \tau_1^{-1} + \tau_2^{-1}, \tag{21a}$$

with

$$\tau_1 = aT \quad \text{and} \quad \tau_2 = \text{const}. \tag{21b}$$

We obtain $a = 7.0 \times 10^{-18}$ s/K and the temperature-independent $\tau_2 = 3.0 \times 10^{-15}$ s. The result of the fit is shown in Fig. 6, together with extrapolations to lower and higher temperatures.

C. The "basic" relaxation mechanism

The fact that all the ${}^{k}\tau_a$ *effectively* fall onto the same line demonstrates that the relaxation of all three nuclei under consideration are governed by the same mechanism, in marked contrast to the standard analysis.

In our model, there exists what we will call a "basic" electronic relaxation mechanism, caused by the spin fluid, that affects the localized moments and exchanges energy with the nuclei. This mechanism is characterized by the short effective correlation time τ_{eff}. In addition, on a long time scale, the spin correlations between these moments vary with the temperature. The observed nuclear spin-lattice relaxation rate ${}^{k}U_{\alpha}$ reflects the temperature dependence of both the basic electronic relaxation and the change in spin correlations. In our model, we can disentangle these two contributions by introducing a basic nuclear relaxation rate ${}^{k}\hat{U}_{\alpha}(T)$, defined by

$${}^{k}\hat{U}_{\alpha}(T) = \frac{{}^{k}V_{\alpha}^{0}}{{}^{k}V_{\alpha}(T)}\,{}^{k}U_{\alpha}(T) = {}^{k}V_{\alpha}^{0}\tau_{eff}(T). \tag{22}$$

The temperature dependence of the basic nuclear rate ${}^{k}\hat{U}_{\alpha}(T)$ is therefore that of the basic electronic relaxation mechanism by definition. Important information about the electronic system is of course also drawn from the temperature dependence of the spin correlation $K_{01}^{\alpha}(T)$ [and hence of ${}^{k}V_{\alpha}(T)$] and will be discussed in Sec. IV F.

From the consistency check Sec. IV B, we therefore conclude that the temperature dependence of the basic relaxation rate (i) is the same for Cu, O, and Y, and (ii) is linear in T at low temperature.

D. Two "basic" electronic relaxation mechanisms

There are four points that now require a discussion—the correlation time τ_1 that dominates the rates ${}^{k}\hat{U}_{\alpha}$ at low tem-

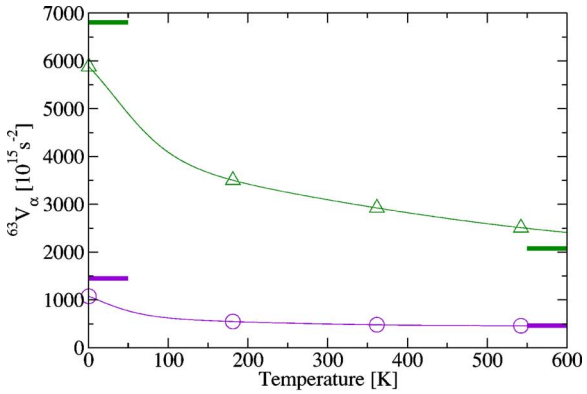

(a) $^{63}V_\alpha$

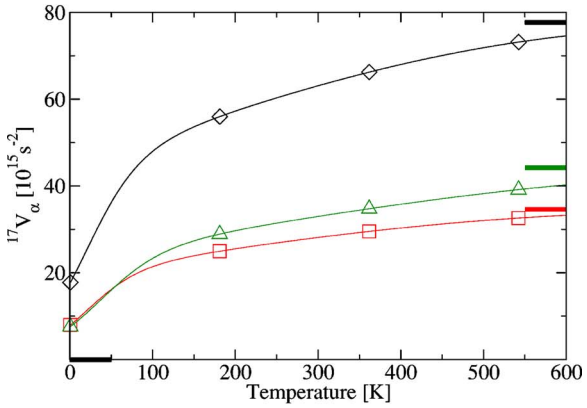

(b) $^{17}V_\alpha$

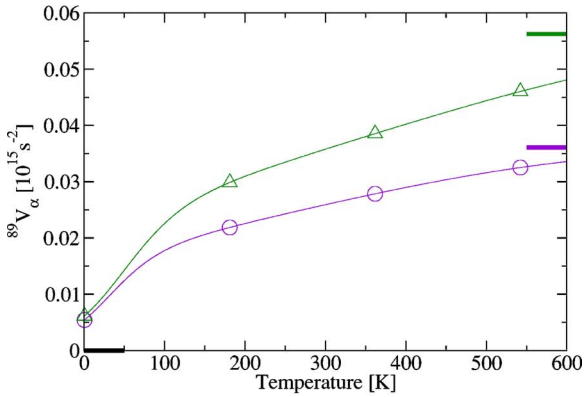

(c) $^{89}V_\alpha$

FIG. 8. (Color online) Temperature dependence of $^kV_\alpha$ in directions a (diamonds), b (squares), ab (circles), and c (triangles), which reflects the change in the degree of coherency. The bars at high temperatures indicate the values $^kV_\alpha^0$ with vanishing correlations; those at $T=0$ indicate the fully correlated values $^kV_\alpha^{fc}$.

peratures, the correlation time τ_2 that dominates at high temperature, the crossover between the two regimes, and the particular form of τ_{eff} [Eq. (21a)], where the rates are combined. There are various possible explanations of the crossover from the initially linear behavior to a saturation at high temperature. We confine ourselves to some basic and simple arguments in order to avoid an overinterpretation at this stage.

We address first the low-temperature regime and consider only the contribution $\tau_1 = aT$. This corresponds to the behavior of T_1^{-1} in a metallic system. Pines and Slichter[30] have discussed magnetic relaxation by fluctuating fields in terms of a random-walk approach and considered also the nuclear relaxation by conduction electrons in metal. Adopting their argument to the present case, the time τ_1 is interpreted as $\tau_1 = p(T)\tau_{dwell}$. This dwelling time $\tau_{dwell} = \hbar/E_F$ is roughly the time a conduction electron spends on a given atom, and $p(T)$ denotes the probability that during τ_{dwell} a nuclear spin-flip occurs. For a degenerate Fermi gas, this probability is $p(T) = T/T_F$, where T_F is the Fermi temperature. With these arguments, we can express our parameter a as

$$a = \frac{\hbar}{k_B T_F^{\,2}}, \tag{23}$$

which yields for the Fermi temperature $T_F = 1050$ K. Moreover, we find then that the residence time on an atom is $\tau_{dwell} = 7.3 \times 10^{-15}$ s. The rather low value[49] of T_F indicates that the degeneracy is lifted. Instead of a well-defined Fermi edge, the distribution is smeared out, and the temperature dependence of the chemical potential becomes important, preventing a quantitative analysis without further information.

Adapting these arguments to the present case, this means that at low temperature, all the spin-lattice relaxation rates (and that also for Cu) in $YBa_2Cu_3O_7$ can be explained by scattering from quasiparticles within a kind of Fermi-liquid model. The influence of the AFM spin correlations is, however, manifest in the temperature-dependent interaction $^kV_\alpha$, whose properties will be investigated in Sec. IV F.

At high temperatures, the data can no longer be explained by a Fermi-liquid behavior, since the influence of the contribution τ_2 grows. According to the fit values, we have $\tau_1 = \tau_2$ at 420 K. We defer a discussion of τ_2 and the crossover τ_1 to τ_2 to later sections, until we have looked at more NMR/NQR data in other cuprates.

As concerns the ansatz (21a) for the effective correlation time, we note that the interactions between the nuclei and the electronic system are the same whatever the basic relaxation mechanisms are. They are determined by the hyperfine energies $^kV_\alpha(T)$, which, however, change from strong AFM correlations at 100 K to weak AFM correlations at around 400 K. Whether we really have two different basic relaxation mechanisms at work or whether they are two different manifestations of the same mechanism is an open question.

A possible explanation for the special form of (21a) is as follows: Adding two rates τ_{short}^{-1} and τ_{long}^{-1} means that the phase correlations between the processes associated with the longer time are destroyed by the impacts of those associated with the shorter time, since immediately after an impact of a process with time τ_{long}, another impact of a process with the short time τ_{short} occurs. In our case, at low temperature $\tau_{short} \equiv \tau_1$ and $\tau_{long} \equiv \tau_2$, and vice versa at high temperature. In addition, we also note that τ_{eff} was originally introduced in Eq. (7) in order to express the time dependence of $\langle S_0^\alpha(t) S_0^\alpha(0)\rangle$. If the time evolution is now governed by two processes so that the Hamiltonian is $\mathfrak{h} = \mathfrak{h}_1 + \mathfrak{h}_2$, we get, in-

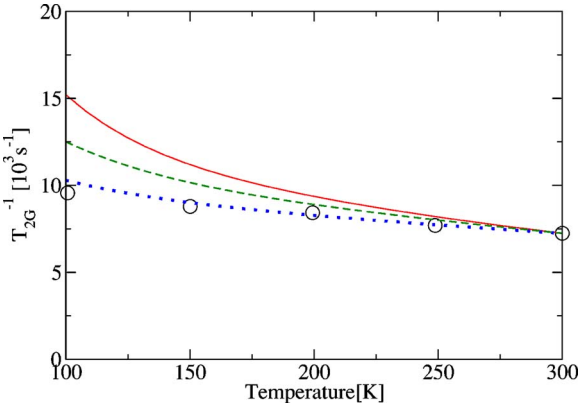

FIG. 9. (Color online) $YBa_2Cu_3O_7$. Comparison with static results (circles) from Imai *et al.* (Ref. 34). All correlations included (full line), only K_{01}^c, K_{01}^c, and K_{01}^c (dashed line), and only NN correlations (dotted line).

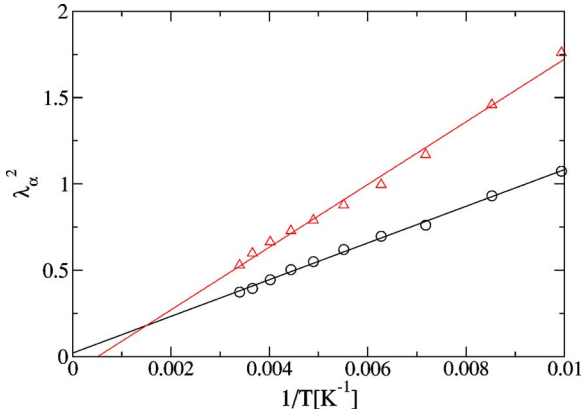

FIG. 10. (Color online) λ_α^2 vs $1/T$ in the direction *ab* (circles) and *c* (triangles). Lines are averages.

stead of Eq. (7), that $\langle S_0^\alpha(t)S_0^\alpha(0)\rangle \propto \exp(-|t|/\tau_1 - |t|/\tau_2)$, provided that $\mathfrak{h}_1$ and $\mathfrak{h}_2$ commute. We see that τ_{eff} would thus be given by Eq. (21a).

E. Comparison of model predictions and measurements at higher temperatures

In $YBa_2Cu_3O_7$, several spin-lattice relaxation rate measurements have been performed at temperatures well above the temperature interval that we used for fitting the model parameters. So far, we have not made use of these data, since they do not allow us to extract the individual contributions ${}^kU_\alpha$. Now, however, it is of interest to compare the extrapolated theoretical predictions with these data. We return to the customary $({}^kT_{1\alpha}T)^{-1}$ representation and show in Fig. 7(a) a plot of $({}^{63}T_{1\alpha}T)^{-1}$ vs T. The high-temperature data of Barrett *et al.*[31] are denoted by triangles pointing down, the original data[8,25] used for the fit below room temperatures are denoted by full circles and full triangles, and the model fit is denoted by the solid line. In Fig. 7(b), we depict the temperature dependence of $({}^{17}T_{1\alpha}T)^{-1}$ and include data points from Nandor *et al.*,[29] who also reported values for $({}^{89}T_{1c}T)^{-1}$, which are shown in Fig. 7(c).

The predictions of the model obtained by extrapolation to higher temperatures are in excellent agreement with the measured relaxation rates of the copper. The downward trend of the relaxation rate of the oxygen is also well reproduced. Less-good agreement is achieved in the case of the yttrium. The experimental rate seems to be more or less constant from 200 K onward, whereas we predict a slowly decreasing rate. This might be due to the simplistic model [Eq. (12)] that we use, neglecting interplane spin correlations and dipolar couplings. We also note that there is some disagreement between the data of Nandor *et al.*[29] and those of Takigawa *et al.*[27] already in the temperature range below 300 K.

On the whole, the model seems to explain the general trends of the data well. A close inspection of the oxygen data, however, shows that the observed increase in the ratio of ${}^{17}T_{1a}^{-1}/{}^{17}T_{1b}^{-1}$ with decreasing temperature reported by Martindale[26] is not reproduced. The increase of the ratio ${}^{17}T_{1c}^{-1}/{}^{89}T_{1c}^{-1}$ for decreasing temperature observed by Takigawa *et al.*[27] is qualitatively reproduced but lacks quantitative agreement. The ratio ${}^{63}T_{1c}^{-1}/{}^{17}T_{1c}^{-1}$ is however in very good agreement with our predictions and will be discussed in Sec. V A.

F. Temperature dependence of interaction energies and the Korringa relation

It is instructive to discuss the calculated values ${}^kV_\alpha(T)$ shown in Fig. 8. The bars on the left in each figure indicate the extremal values ${}^kV_\alpha^0$ [Eq. (16)] if the system was fully antiferromagnetic. The bars on the right show the other extreme ${}^kV_\alpha^0$ [Eq. (15)], for a system with no correlations remaining. In the case of the oxygen [Fig. 8(b)], ${}^{17}V_\alpha(T) = {}^{17}V_\alpha^0(1-|K_{01}^\alpha(T)|)$ increases with T for all directions α since the spin correlations tend to zero. For the copper [Fig. 8(a)], ${}^{63}V_\alpha(T)$ drops with increasing temperature, since the values of the hyperfine interactions incidentally are such that the values for fully AFM correlations ${}^{63}V_\alpha^{fc}$ (bars on the left) are higher than for no correlations ${}^{63}V_\alpha^0$ (bars on the right). Note that this is the case for both directions α parallel and perpendicular to the planes. The different temperature dependencies of the rates measured at the copper and at the oxygen thus find a straightforward explanation. While the basic relaxation rates are identical for both nuclei, ${}^{63}V_\alpha(T)$ has a temperature behavior opposite to ${}^{17}V_\alpha(T)$ due to the particular values of the hyperfine interaction energies, which are atomic properties.

The temperature dependencies of the rates ${}^kU_\alpha$ result from a delicate balance between ${}^kV_\alpha$ and $\tau_{eff}(T)$. From 100 K to 300 K, τ_{eff} increases by about 170%, whereas ${}^{63}V_c$ drops by 24%, but ${}^{17}V_a$ increases by 32%. Some ${}^kV_\alpha$ values depend crucially on the precise values of the hyperfine energies. Moreover, the rates ${}^kT_{1\alpha}^{-1}$ that are directly accessible by experiments are linear combinations of the ${}^kU_\alpha$. It is, therefore, important to study in detail the interplay between $\tau_{eff}(T)$ and ${}^kV_\alpha(T)$.

We illustrate in Appendix B the various contributions to ${}^{63}V_\alpha(T)$ and discuss the interplay between nearest and farther-distant AFM spin correlations. At this point, we just

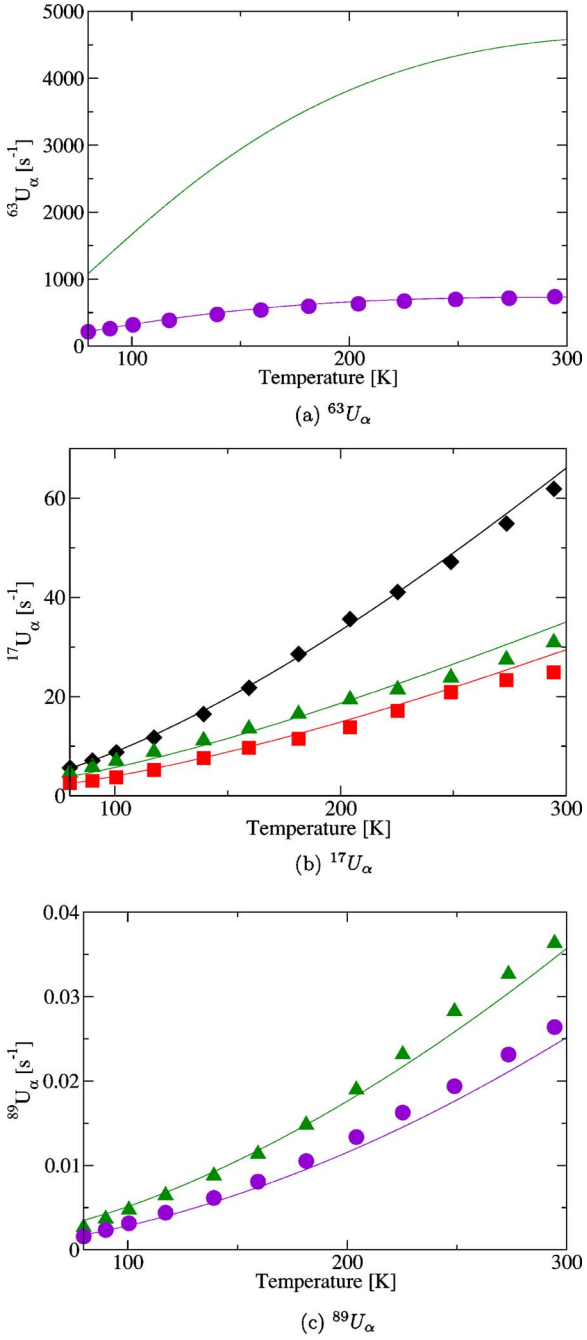

FIG. 11. (Color online) $YBa_2Cu_3O_{6.63}$. Symbols are experimental data; lines denote the fit as explained in the text. Directions *a* (diamonds), *b* (squares), *ab* (circles), and *c* (triangles).

note that in the framework of the MMP model, the Fermi-liquid contribution that dominates the relaxation rates of the oxygen and yttrium contains no correlations, i.e., would correspond to ${}^kV_\alpha^0$ (shown by the high temperature bars in Fig. 8).

It seems now also appropriate to comment on the Korringa relation, which has been discussed in numerous publications on NMR data analysis in cuprates. The original Korringa relation has been derived for an isotropic system. To obtain a similar relation for layered materials would require (i) temperature independent ${}^kV_\beta$ and ${}^kV_\gamma$ and a $\tau_{eff}(T)$ that is

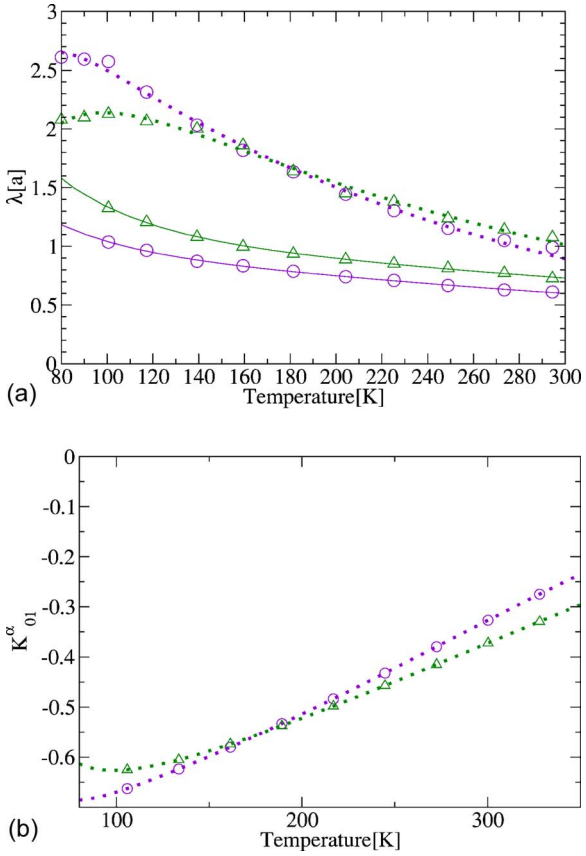

FIG. 12. (Color online) Correlation lengths and correlations in $YBa_2Cu_3O_{6.63}$. (a) λ_{ab} (circles) amd λ_c (triangles); $YBa_2Cu_3O_7$ (solid lines) and $YBa_2Cu_3O_{6.63}$ (dotted lines). (b) K_{01}^{ab} (circles) and K_{01}^c (triangles) in $YBa_2Cu_3O_{6.63}$.

proportional to T and to ρ^2, the square of the density of states at the Fermi surface; (ii) a temperature-independent static spin susceptibility in direction α; or (iii) an incidental cancellation of the corresponding temperature dependencies in all these quantities, which in the frame of the present model and in view of Eq. (23) and Fig. 8 is very unlikely. From these considerations, we conclude that looking for and discussing Korringa relations for NMR data in layered cuprates is probably highly questionable.

In Appendix B, we show how an apparent linear temperature dependence of the oxygen relaxation rate may occur in a limited temperature interval.

G. Spin-spin relaxation

It is worthwhile at this stage to connect the present model for the spin-lattice relaxation in cuprates with the theory and experiments of the nuclear spin-spin relaxation rate T_{2G}^{-1} that have been put forward by Slichter and co-workers.[32–35] T_{2G}^{-1} measures the strengths of the indirect nuclear spin-spin interaction mediated by the nonlocal static spin susceptibility $\chi'(\vec{r})$.

Imai *et al.*[33] pointed out the importance of T_{2G}^{-1} to obtain information about the AFM exchange between the electron spins. They demonstrated that low-field NMR measurements of ${}^{63}T_{2G}^{-1}$ give a strong quantitative constraint on $\chi'(\vec{q})$ in

cuprates. They discovered that the staggered susceptibility $\chi'(\vec{Q})$ follows a Curie-Weiss law in $YBa_2Cu_3O_7$.

Since Haase *et al.*[35] also presented a derivation of $\chi'(\vec{r})$ in direct space, it is of interest to compare Eq. (6) in Ref. 35 with our expression (14b) for ${}^{63}V_c(T)$. The functional form is the same, but we note that ${}^{63}T_{2G}^{-1}$ requires the knowledge of the correlations at any distance $\vec{r}$, whereas ${}^{63}V_c$ contains only the closest correlations. From the fit of the relaxation-rate data, we got values for K_{01}^{α}, K_{12}^{α}, and K_{13}^{α}, which, by assumption, could be provided by a static spin susceptibility

$$\chi'_{\alpha}(\vec{r}) \propto \cos(\vec{Q}\cdot\vec{r})e^{-r/\lambda_{\alpha}}. \tag{24}$$

We have, however, no information about $\chi'_{\alpha}(\vec{r})$ for $|\vec{r}|<1$ and for $|\vec{r}|>2$. Nevertheless, the Fourier transform at $\vec{q}=\vec{Q}$ gives

$$\chi'_{\alpha}(\vec{Q}) = 2\pi\lambda_{\alpha}^2 E\chi'_{\alpha}(\vec{q}=0), \tag{25}$$

where E is an enhancement factor that, in the present approach, cannot be determined [expression (25) compares to the isotropic $\chi'(\vec{Q})=\alpha\xi^2$ in the MMP model[16]]. Assuming that Eq. (24) also applies to correlations at arbitrary distances, we evaluate ${}^{63}T_{2G}^{-1}$ using the values $\lambda_c(T)$ obtained from the analysis of the ${}^{k}T_{1\alpha}^{-1}$ (Sec. IV A). The resulting temperature dependence is shown in Fig. 9 (solid line), together with the data from Imai *et al.*[34] (circles). $F:=E\chi'(\vec{r}=0)/\mu_B^2$ was taken in (25) as a parameter to adjust, and we calculated it so that our result at $T=300$ K corresponds to the data. We found in this case $F=8.0\ \mathrm{eV}^{-1}$. Our prediction of the temperature dependence deviates from the measurements, which may indicate that our assumption of an exponential decay of $\chi'(\vec{r})$ overemphasizes the contributions of high-order correlations. If we drop all the correlations except those coming into the ${}^{k}T_{1\alpha}^{-1}$—that is, K_{01}^{c}, K_{12}^{c}, and K_{13}^{c}—we get the dashed line in Fig. 9 with $F=8.6\ \mathrm{eV}^{-1}$. A better correspondence with the data is obtained if we only keep K_{01}^{c} (dotted line), where then $F=11.1\ \mathrm{eV}^{-1}$.

On the whole, these results are in agreement with those obtained by Imai *et al.*,[33,34] who utilized a Gaussian form for the q dependence of $\chi'(\vec{q})$ near $\vec{q}=\vec{Q}$. In this work, we have used a different parametrization of the AFM correlations (which yields shorter correlation lengths), but it seems worthwhile to test further the implications of the present model on $\chi'(\vec{Q})$. An inspection of Eq. (25) shows that the increase of λ_{α}^2 with decreasing temperature determines the increase of staggered susceptibility, provided that $E\chi'(\vec{q}=0)$ is temperature independent. In Fig. 10, we plotted the λ_{α}^2 vs $1/T$ as we obtained them in Sec. IV A from the fit on all spin-lattice relaxation data. It is surprising how well these values obey a Curie (or Curie-Weiss) behavior. It seems that upon cooling, the spins in $YBa_2Cu_3O_7$ remember their tendency to align antiferromagnetically, but they are prevented from doing so as the more energetically favored superconductivity sets in. This feature has been observed and discussed by Imai *et al.*[33,34]

An important question at this stage is whether those AFM correlations persist in the superconducting state. There are strong indications that the correlations develop an extreme anisotropy[36] below T_c. The question of the persistence of correlations in this state will reveal extremely interesting information about the interplay of magnetism and superconductivity, which, however, is not the focus of the present work.

V. UNDERDOPED YBCO COMPOUNDS

In this section, the model is applied to analyze NMR and NQR experiments in $YBa_2Cu_3O_{6.63}$ and in $YBa_2Cu_4O_8$. We do not have for these compounds the same full set of data as for the optimally doped $YBa_2Cu_3O_7$, and we therefore restrict our analysis to exploring the general trends of the doping and temperature dependencies of the AFM correlations and the effective correlation time τ_{eff}. We retain the same hyperfine interaction energies that have been determined for $YBa_2Cu_3O_7$ in the analysis of $YBa_2Cu_3O_{6.63}$ and even for $YBa_2Cu_4O_8$. In the latter case, we are able to compare our model predictions with high-temperature measurements.

A. $YBa_2Cu_3O_{6.63}$

To determine the rates ${}^{k}U_{\alpha}$, we used the following published spin-lattice relaxation data: the copper data from Takigawa *et al.*[12] (only providing ${}^{63}T_{1c}^{-1}$), the oxygen data ${}^{17}T_{1\alpha}^{-1}$ taken from Martindale *et al.*,[26] and the yttrium data ${}^{89}T_{1\alpha}^{-1}$ from Takigawa *et al.*[27] They cover the temperature range from T_c up to room temperature. We are not aware of measurements at elevated temperatures. The resulting relaxation rates ${}^{k}U_{\alpha}$ are shown (symbols) in Fig. 11. The lines in this figure will be explained later. A comparison with those of the optimally doped material (Fig. 1) reveals that now the temperature dependencies deviate more strongly from a linear behavior with a convex (concave) curvature for ${}^{63}U_{\alpha}(T)$ $[{}^{17}U_{\alpha}(T)]$, but we do not consider this to be a dramatic contrast.

The same fitting procedure explained in Sec. IV A was then carried out, except that the values for the hyperfine interaction energies were kept fixed at the optimized values found for $YBa_2Cu_3O_7$ (Table I). It is therefore expected that the quality of the fit will be less good than for $YBa_2Cu_3O_7$. The result is depicted in Fig. 12(a), which shows the temperature dependence of the correlation lengths λ_{α} compared with the values for the optimally doped material. As expected, the values for λ_{α} are higher (by about a factor of 2) in the underdoped compound but exhibit a peculiar crossover when the temperature drops below 100 K. In this region, we also get $\lambda_c<\lambda_{ab}$. Whether this behavior is physically really significant or just shows the inadequacy of the postulated model is undetermined. As was done for $YBa_2Cu_3O_7$, the correlation lengths can be fitted with a sum of exponential functions. The correlations built using the exponential fit are plotted in Fig. 12(b). For completeness, we have plotted in Fig. 13 the calculated ${}^{k}V_{\alpha}$.

The consistency check in analogy with Sec. IV B gives six different values for ${}^{k}\tau_{\alpha}(T)$, which are gathered in Fig. 14. Although this time, the spread among the different values is considerably larger than that for $YBa_2Cu_3O_7$ (see Fig. 5), the agreement is still surprisingly good. The temperature depen-

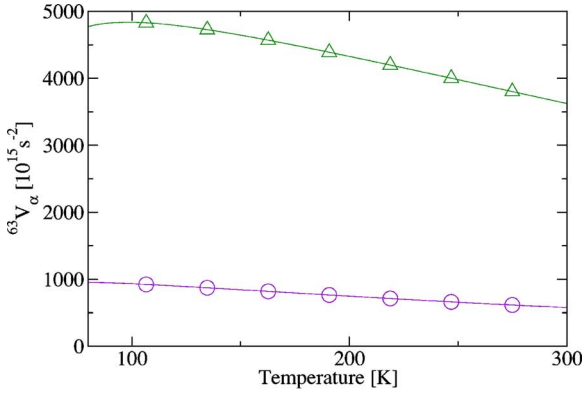

(a) $^{63}V_\alpha$

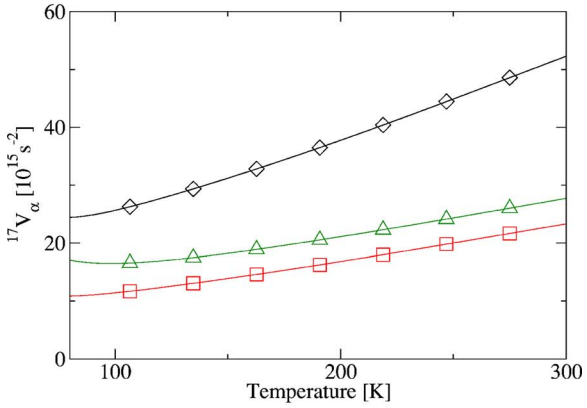

(b) $^{17}V_\alpha$

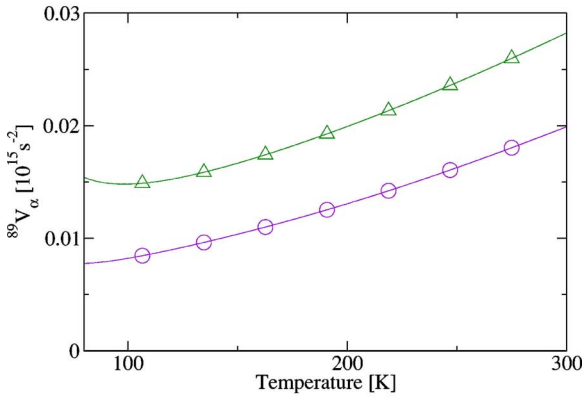

(c) $^{89}V_\alpha$

FIG. 13. (Color online) $YBa_2Cu_3O_{6.63}$. Calculated $^kV_\alpha$, in the directions *a* (diamonds), *b* (squares), *ab* (circles), and *c* (triangles).

dence of the calculated mean values (circles in Fig. 14) could not be fitted with the function (21a). However, the same ansatz,

$$\tau_{eff}^{-1} = \tau_1^{-1} + \tau_2^{-1}, \tag{26a}$$

but with

$$\tau_1 = aTe^{-g/T} \quad \text{and} \quad \tau_2 = \text{const}, \tag{26b}$$

provides a very good fit (as shown in Fig. 15) with the values $a = 10 \times 10^{-18}$ s/K, $g = 97$ K, and $\tau_2 = 2.9 \times 10^{-15}$ s.

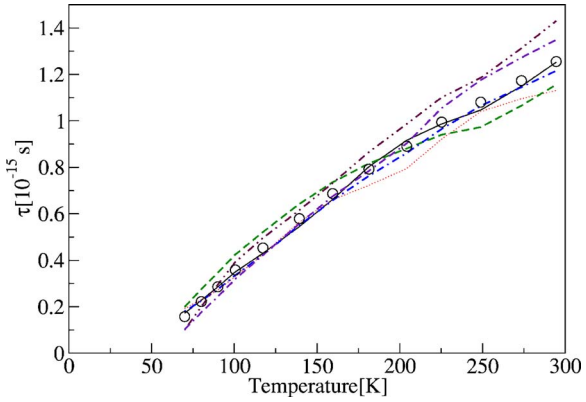

FIG. 14. (Color online) τ_{eff} in $YBa_2Cu_3O_{6.63}$ obtained from a λ minimization at the optimized parameters (Table I). The circles are the calculated average; $^{17}\tau_a$ (thin solid line), $^{17}\tau_b$ (thin dotted line), $^{17}\tau_c$ (thin dashed line), $^{63}\tau_{ab}$ (thick dashed-dotted line), $^{89}\tau_{ab}$ (thick dash-dot-dot-dashed line), and $^{89}\tau_c$ (thick dot-dash-dash-dotted line).

The lines in Fig. 11 show the model-calculated *U*'s compared with the experiments, whereas Fig. 16 depicts the data and the fit in the usual $(^kT_{1\alpha}T)^{-1}$ vs T representation. The agreement is now only approximate but could be improved by further adjustments (in particular, the hyperfine field constants) and weighting of the data according to their precision. A further confirmation that the fit is, however, convincing is given in Fig. 17, where we have plotted the ratio $^{63}T_{1c}^{-1}/^{17}T_{1c}^{-1}$. On top of our original data (stars and plus signs) and our model predictions (solid and dotted lines), we also show the data (squares) obtained by combining the high-temperature $YBa_2Cu_3O_7$ measurements of Barrett *et al.*[31] and Nandor *et al.*[29] already discussed in Sec. IV E. At high temperature, we expect the AFM correlations to become negligible. In this case, the hyperfine fields must be fully uncorrelated, and the ratio $^{63}T_{1c}^{-1}/^{17}T_{1c}^{-1}$ tends to $(A_{ab}^2+4B^2)/(C_a^2+C_b^2)$, which is about 8.2. This value is denoted by a dotted line in Fig. 17. As can be seen in that figure, the high-temperature data confirm this prediction, which is a known result for the relaxation by randomly fluctuating hyperfine fields.

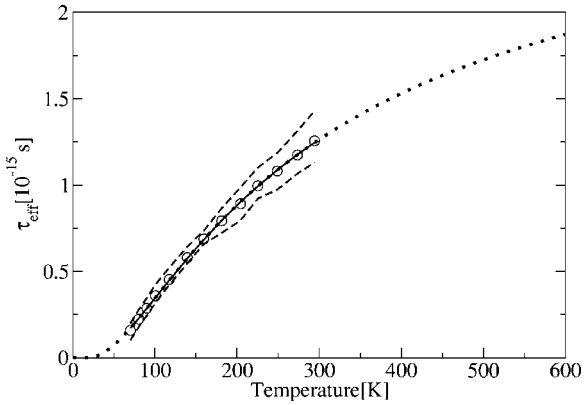

FIG. 15. τ_{eff} in $YBa_2Cu_3O_{6.63}$ obtained from a λ minimization at the optimized parameters. The circles are the calculated average, and the dashed lines are the upper and lower bounds. The solid line is the fit as explained in the text.

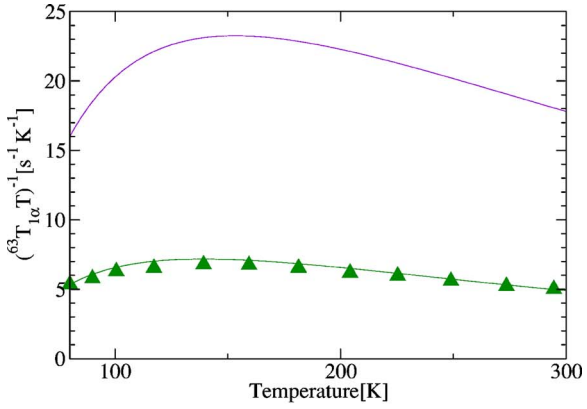

(a) $(^{63}T_{1\alpha}T)^{-1}$

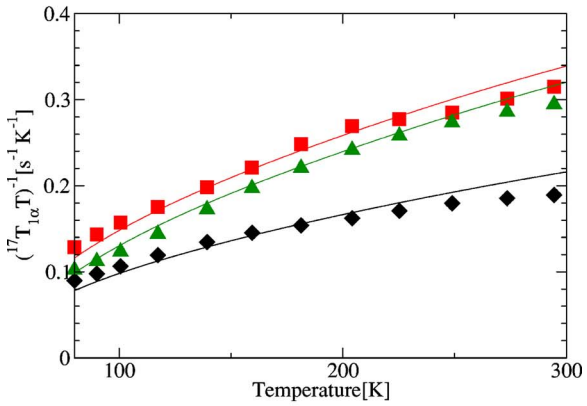

(b) $(^{17}T_{1\alpha}T)^{-1}$

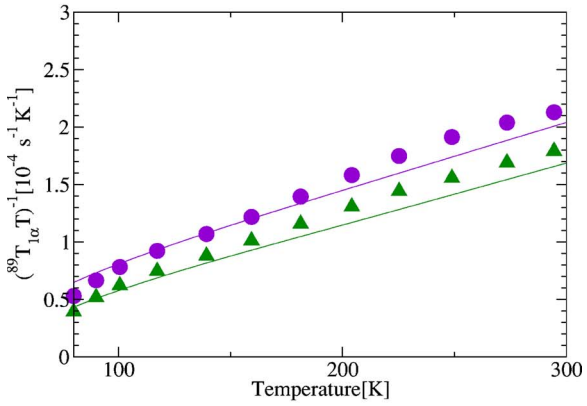

(c) $(^{89}T_{1\alpha}T)^{-1}$

FIG. 16. (Color online) $YBa_2Cu_3O_{6.63}$. Symbols are experimental data, and lines are the fit as explained in the text. Directions *a* (diamonds), *b* (squares), *ab* (circles), and *c* (triangles).

B. $YBa_2Cu_4O_8$

In stoichiometric $YBa_2Cu_4O_8$, NMR and NQR lines are much narrower than in other cuprates and allow precise measurements. Raffa *et al.*[37] reported high-accuracy ^{63}Cu NQR spin-lattice relaxation measurements on ^{16}O- and ^{18}O-exchanged samples of $YBa_2Cu_4O_8$. They analyzed their data with the help of the phenomenological relation

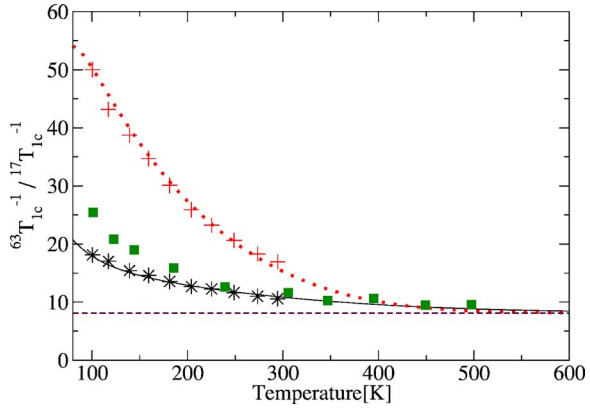

FIG. 17. (Color online) $^{63}T_{1c}^{-1}/^{17}T_{1c}^{-1}$ in $YBa_2Cu_3O_7$ (stars) and $YBa_2Cu_3O_{6.63}$ (plus signs). The squares are experimental data as cited in the text. The solid and dotted lines are the predictions derived from the model, and the dashed line is the expected value in the absence of AFM correlations.

$$(^{63}T_{1c}T)^{-1} = CT^{-a}\left[1 - \tanh^2\left(\frac{\Delta}{2T}\right)\right], \tag{27}$$

which worked reasonably well. To investigate a possible isotope effect of the spin gap parameter Δ, they could considerably improve the agreement between data and fit function by slightly adjusting the temperature dependence of the function (27).

In terms of our model, the temperature dependence of the relaxation rate is given by

$$^{63}T_{1c}^{-1} = 2\,^{63}U_{ab}(T) = 2\,^{63}V_{ab}(T)\tau_{eff}(T). \tag{28}$$

To test the quality of the ansatz (26a) for the combined effective correlation time, we simply take the values for the $^{63}V_{ab}(T)$ that we have extracted for the $YBa_2Cu_3O_7$ system. Equation (28) is then used to determine the $\tau_{eff}(T)$ from the data of Raffa *et al.*[37] The data (for the ^{16}O sample) and the fit are shown in Fig. 18(a). Figure 18(b) shows the same data with the calculated values extrapolated outside the range ($100\ \mathrm{K} < T < 310\ \mathrm{K}$), and with the addition of high-temperature data from Curro *et al.*[38] and Tomeno *et al.*[39] The temperature dependence of τ_{eff} is represented in Fig. 19. The fit gives $a = 44 \times 10^{-18}$ s/K, g = 195 K, and $\tau_2 = 1.9 \times 10^{-15}$ s. Note that these values will change if the $^{63}V_{ab}(T)$ values appropriate to $YBa_2Cu_4O_8$ (which are expected to be somewhat larger between 100 K and 300 K due to enhanced correlations) can be extracted. We guess that our ansatz (26a) might find a better physical motivation than (27). Moreover, the fit is excellent and the extrapolation to higher temperatures is in addition in good agreement with the data available.

VI. LASCO COMPOUNDS

A large amount of NMR and NQR data exist also for $La_{2-x}Sr_xCuO_4$ for various doping levels x. Mostly, relaxation rates have been reported for $^{63}T_{1c}^{-1}$, with only few measurements for the oxygens. Haase *et al.*[40] have been able to determine $K_{01}(T)$ [$\rho_{01}(T)$ in their work] from the linewidth of

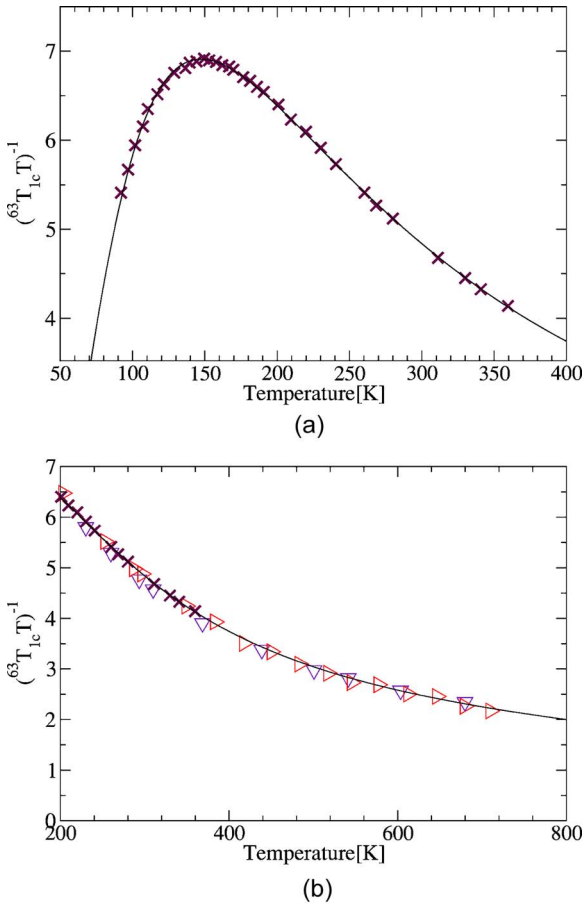

FIG. 18. (Color online) (a) Data from Raffa *et al.* (Ref. 37) (crosses) and fit as described in the text (solid line). (b) Extrapolation of fit to higher temperatures and data from Curro *et al.* (Ref. 38) (triangles pointing right) and Tomeno *et al.* (Ref. 39) (triangles pointing down).

apical, planar O and Cu in $La_{2-x}Sr_xCuO_4$. For the optimally doped compound, they find that the correlation decreases with the temperature and is about −0.4 at room temperature. The correlations are of course expected to be large for low doping. In the framework of our model, we are not in a

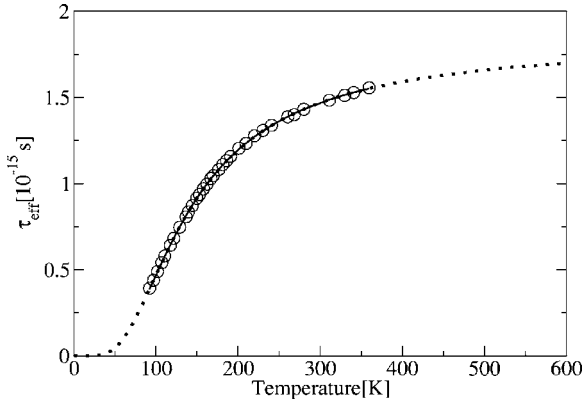

FIG. 19. τ_{eff} (circles) is obtained from $^{63}V_{ab}(T)$ and the data from Raffa *et al.* (Ref. 37). Dotted line denotes the fit as described in the text.

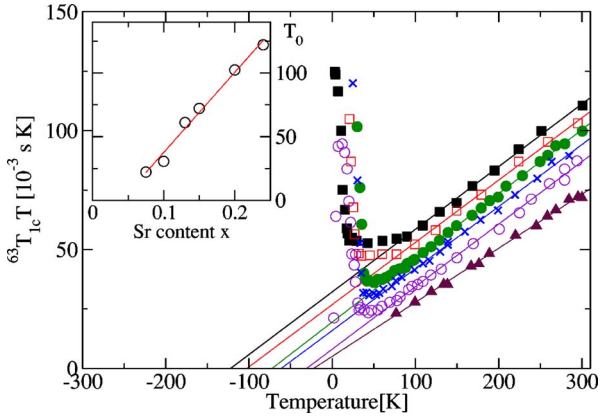

FIG. 20. (Color online) $^{63}T_{1c}T$ vs T plot with the data from Ohsugi *et al.* (Ref. 41) for $La_{2-x}Sr_xCuO_4$. $x=0.24$ (solid squares), $x=0.2$ (open squares), $x=0.15$ (solid circles), $x=0.13$ (crosses), $x=0.1$ (open circles), and $x=0.075$ (solid triangles). In the inset, T_0 is plotted vs the strontium concentration.

position to determine the correlation lengths λ_{ab} and λ_c since we do not have enough data. We therefore restrict ourselves in this section to a more qualitative discussion of the temperature dependence of $^{63}T_{1c}^{-1}$. In particular, we can compare the high-temperature limit of the effective correlation time τ_2 to the relaxation mechanism of local magnetic moments in a paramagnet.

We reproduce in Fig. 20 the measurements of Ohsugi *et al.*,[41] who present their data in a $^{63}T_{1c}T$ vs T plot.

The straight lines that fit the data well at temperatures above 100 K correspond to

$$^{63}T_{1c}T = \alpha + \alpha T/T_0 \tag{29}$$

and lead, in analogy to the Curie-Weiss law for the susceptibility in insulating antiferromagnets, to the notion of Curie-Weiss behavior of $(^{63}T_{1c}T)^{-1}$.

In our model, we also expect to find for $La_{2-x}Sr_xCuO_4$ a τ_{eff} as given by Eqs. (26), that is

$$^{63}T_{1c}T = \frac{1}{2^{63}V_{ab}(T)}\left(\frac{1}{a}e^{g/T} + \frac{T}{\tau_2}\right). \tag{30}$$

At high temperatures, the AFM correlations vanish, $^{63}V_{ab}$ is temperature independent, and $T \gg g$. We find indeed in this case a linear T dependence and can identify

$$\alpha \equiv \frac{1}{2^{63}V_{ab}^0 a} \quad \text{and} \quad T_0 \equiv \frac{\tau_2}{a}. \tag{31}$$

It is surprising, however, that this linear temperature dependence dominates already at $T \gtrsim 100$ K. It is probable that, like in $YBa_2Cu_3O_7$, the temperature dependence of $^{63}V_{ab}$ is weak. We show in Appendix B that due to the incidental values of the hyperfine energies for copper, a cancellation of contributions from NN and farther-distant correlations occurs.

Imai *et al.*[42] have studied $La_{2-x}Sr_xCuO_4$ by NQR up to high temperatures and found two striking results. First, at high temperatures (~600 K), the $^{63}T_{1c}^{-1}$ rates of all samples

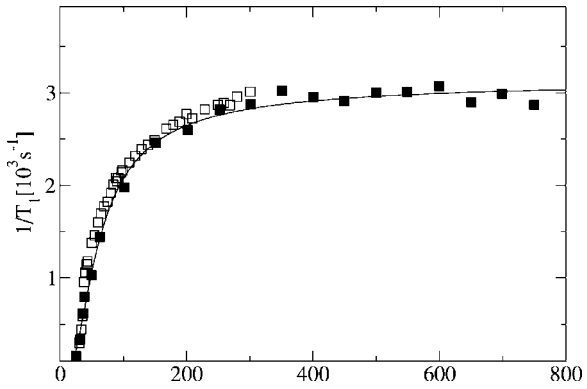

FIG. 21. $La_{2-x}Sr_xCuO_4$ data from Imai *et al.* (Ref. 42) (solid squares) and Ohsugi *et al.* (Ref. 41) (for $x=0.15$; open squares).

(with doping levels $x=0$, 0.02, 0.04, 0.045, 0.075, and 0.15) were nearly identical, although the system with $x=0$ is an insulator and its magnetic behavior can well be described by a two-dimensional Heisenberg antiferromagnet, whereas the samples with $x=0.075$ and 0.15 are conducting and, at low T, even superconducting. Second, they observed that at high temperatures, ${}^{63}T_{1c}$ becomes independent of temperature.

The first striking result of Imai *et al.*,[42] that is, the nearly identical values of ${}^{63}T_{1c}^{-1}$ for $x=0$ up to $x=0.15$, is a strong argument for identifying τ_2 as a time scale dictated by the dynamics of the antiferromagnetism that persists well into the doped and overdoped region. This can be illustrated as follows. Moriya[43] has calculated T_1^{-1} for a nucleus of a magnetic ion in an *insulating* antiferromagnet. In the paramagnetic regime, Moriya treated the exchange interaction within the model of a Gaussian random process with correlation frequency ω_e. This was adapted by Imai *et al.*[42] to a square lattice and appropriate hyperfine interaction energies for pure La_2CuO_4 with the result [Eq. (4) in Ref. 42]

$$ {}^{63}T_{1\infty}^{-1} = \sqrt{2\pi}(A_{ab}^2 + 4B^2)\frac{1}{4\hbar^2\omega_e'}, \tag{32}$$

where $\omega_e' = \omega_e[2A_{ab}B/(A_{ab}^2+4B^2)]^{1/2}$ slightly modifies ω_e ($\omega_e' \approx 0.9\omega_e$).

In the limit of high temperature, our model simplifies to

$$ \lim_{T\to\infty} {}^{63}T_{1c}^{-1} = 2\,{}^{63}V_{ab}^0\tau_2 = \frac{2}{4\hbar^2}(A_{ab}^2 + 4B^2)\tau_2, \tag{33}$$

and, therefore, the relation

$$ \tau_2 = \sqrt{\frac{\pi}{2}}\frac{1}{\omega_e'} \tag{34}$$

connects our correlation time τ_2 to the correlation frequency of a magnetic moment in the paramagnetic regime of an insulating antiferromagnet. It must be stressed, however, that in the present work, the time τ_2 had been introduced as an independent contribution to $\tau_{eff}(T)$, i.e., $\tau_{eff}^{-1} = \tau_1^{-1} + \tau_2^{-1}$, which gave an excellent fit to the relaxation rate data in *metallic* $YBa_2Cu_3O_7$ for 100 K $<$ T $<$ 300 K, with τ_1 linear in T and τ_2 constant.

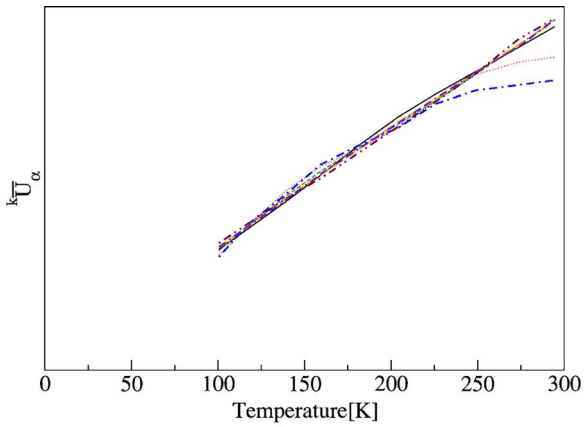

(a) $YBa_2Cu_3O_7$

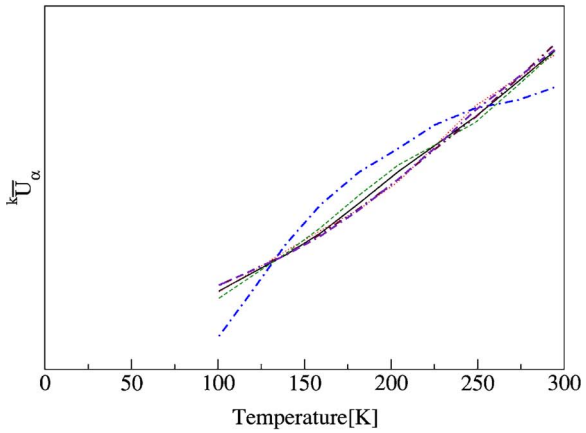

(b) $YBa_2Cu_3O_{6.63}$

FIG. 22. (Color online) The ${}^kU_\alpha$ after affine transformations of the data. ${}^{17}\bar{U}_a$ (thin solid line), ${}^{17}\bar{U}_b$ (thin dotted line), ${}^{17}\bar{U}_c$ (thin dashed line), ${}^{63}\bar{U}_{ab}$ (thick dashed-dotted line), ${}^{63}\bar{U}_c$ (thick dashed line), ${}^{89}\bar{U}_{ab}$ (thick dash-dot-dot-dashed line), and ${}^{89}\bar{U}_c$ (thick dot-dash-dash-dotted line).

To complement these qualitative findings with a quantitative result, we present in Fig. 21 the data reported by Imai *et al.*[42] (solid squares) and Ohsugi *et al.*[41] (open squares) for the $x=0.15$ samples together with a fit of the data from the former source, according to (26a). The fit, for which we have assumed a constant value for ${}^{63}V_{ab}^0$, gives ${}^{63}V_{ab}^0 a = 57.1$ (sK)$^{-1}$, ${}^{63}V_{ab}^0\tau_2 = 1574$ s^{-1}, and $g=64.1$ K. Adopting the hyperfine interaction energies for La_2CuO_4 reported by Haase *et al.*,[44] we find $a = 106\times10^{-18}$ s/K and $\tau_2 = 2.92\times10^{-15}$ s. It is interesting to note that this value of τ_2 is very close to those obtained for $YBa_2Cu_3O_7$ and $YBa_2Cu_3O_{6.63}$.

VII. SUMMARY AND CONCLUSIONS

We have compiled a complete set of relaxation rate data for optimally doped $YBa_2Cu_3O_7$ from T_c up to room temperature and extracted ${}^kU_\alpha$, the contributions to the rates from the fluctuations along the individual crystallographic axes. The result of this simple data transformation is that,

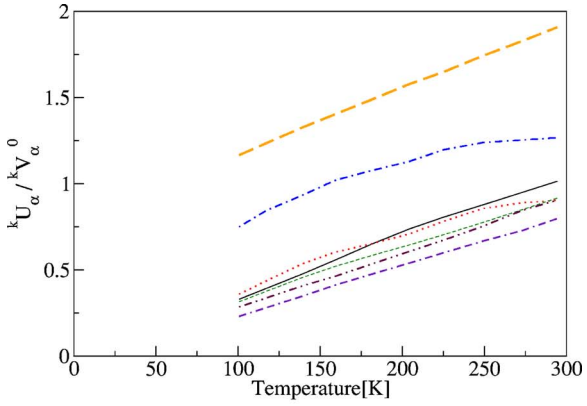

(a) $YBa_2Cu_3O_7$

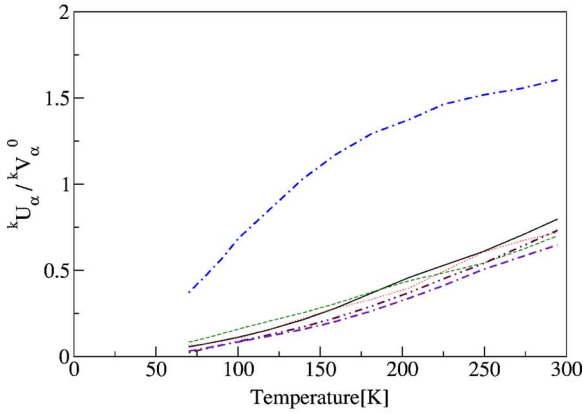

(b) $YBa_2Cu_3O_{6.63}$

FIG. 23. (Color online) ${}^k\tilde{U}_\alpha(T) = {}^kU_\alpha(T)/{}^kV_\alpha^0$. ${}^{17}\tilde{U}_a$ (thin solid line), ${}^{17}\tilde{U}_b$ (thin dotted line), ${}^{17}\tilde{U}_c$ (thin dashed line), ${}^{63}\tilde{U}_{ab}$ (thick dashed-dotted line), ${}^{63}\tilde{U}_c$ (thick dashed line), ${}^{89}\tilde{U}_{ab}$ (thick dash-dot-dot-dashed line), and ${}^{89}\tilde{U}_c$ (thick dot-dash-dash-dotted line).

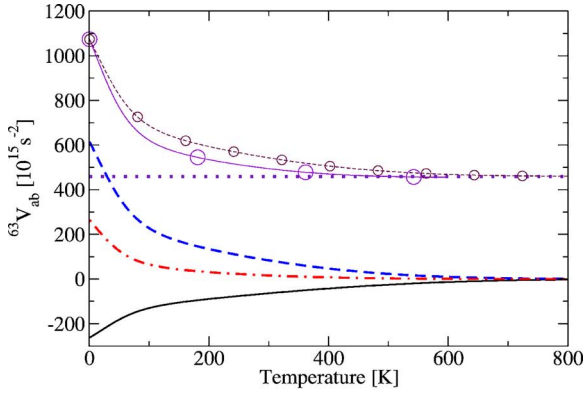

(a) Decomposition of ${}^{63}V_{ab}$

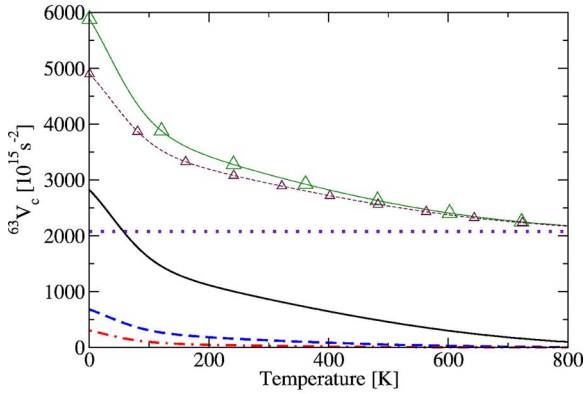

(b) Decomposition of ${}^{63}V_c$

FIG. 24. (Color online) $YBa_2Cu_3O_7$. Full ${}^{63}V_\alpha$ (large circles), ${}^{63}V_\alpha^0$ (dotted line), ${}^{63}V_\alpha^1$ (solid line), ${}^{63}V_\alpha^2$ (dashed line), and ${}^{63}V_\alpha^3$ (dashed-dotted line). ${}^{63}V_{ab}^0 + {}^{63}V_{ab}^2$ (small circles) and ${}^{63}V_c^0 + {}^{63}V_c^1$ (small triangles).

from this point of view, there is no striking difference between the copper and the oxygen relaxations. This suggested the decoupling ${}^kU_\alpha(T) = {}^kV_\alpha(T)\tau_{eff}(T)$, where the temperature dependence of ${}^kV_\alpha$ is given by the static AFM correlations $K_{01}^\alpha(T)$ for the oxygen and $K_{01}^\alpha(T)$, $K_{12}^\alpha(T)$, and $K_{13}^\alpha(T)$ for the copper. A numerical fit to the data on τ_{eff}-independent ratios of relaxation rates yielded the correlation lengths as a function of the temperature as well as refined hyperfine field constants. The validity of our approach is confirmed by the fact that the seven ${}^k\tau_\alpha(T)$ are well grouped. The average, assimilated to the effective correlation time τ_{eff}, is extremely well modeled by $\tau_{eff}^{-1}(T) = \tau_1^{-1}(T) + \tau_2^{-1}$, with τ_2 constant and $\tau_1(T)$ linear in T. This led to the surprising result that in $YBa_2Cu_3O_7$, the basic relaxation of all three nuclei under consideration is dominated at low temperature by scattering processes of fermionic excitations. The extrapolation of the model predictions to higher temperatures is in very good agreement with the measurements. A similar but slightly reduced analysis was conducted on $YBa_2Cu_3O_{6.63}$, leading as expected to higher values for the correlations. In the case of $YBa_2Cu_4O_8$, we had an even more reduced set of data; however, some very precise data for Cu are available at high temperature. The analysis of the effective correlation time $\tau_{eff}(T)$ in both underdoped compounds revealed that $\tau_{eff}^{-1}(T) = \tau_1^{-1}(T) + \tau_2^{-1}$ fits the result again very well, provided that $\tau_1(T)$ is modified by a gap function at lower temperature. From the analysis of the $La_{2-x}Sr_xCuO_4$ series, we could connect τ_2 with relaxation due to AFM spin fluctuations in a paramagnetic state.

In conclusion, we have shown that in the model of fluctuating fields, the AFM spin-spin correlations $K_{01}^\alpha(T)$, $K_{12}^\alpha(T)$, and $K_{13}^\alpha(T)$ determine the degree of coherency. In our fit to the data, we found that the in-plane correlations are about -0.4 for $YBa_2Cu_3O_7$ and -0.65 for $YBa_2Cu_4O_8$ at 100 K. The copper and yttrium relaxation rates depend on all three correlations $K_{01}^\alpha(T)$, $K_{12}^\alpha(T)$, and $K_{13}^\alpha(T)$, whereas ${}^{17}T_{1\alpha}^{-1}$ involves only K_{01}^α. Moreover, the contributions of the three correlations at the copper partially cancel out due to the particular values of the hyperfine field constants. It would be therefore extremely useful to collect more measurements on oxygen, in all crystallographic directions and in all substances.

We also note that whereas the particular choice of spatial exponential decay of the correlations fixes the details of the

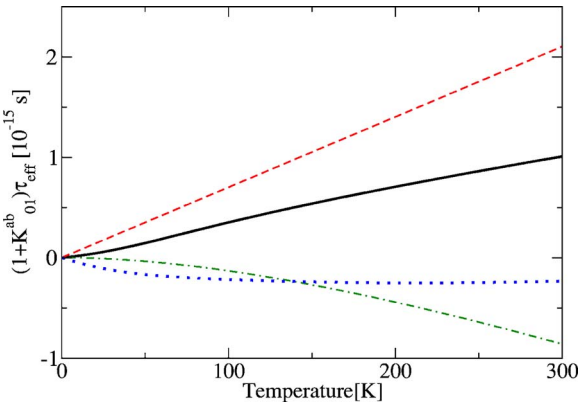

FIG. 25. (Color online) $YBa_2Cu_3O_7$. Decomposition of $(1+K_{01}^{ab})\tau_{eff}$ (solid line)—τ_1 (dashed line), $\tau_{eff}-\tau_1$ (dashed-dotted line), and $K_{01}^{ab}\tau_{eff}$ (dotted line).

correlation lengths and hyperfine field constants, the same general conclusions of our model would be drawn if another form of spatial decay were applied. Another note is that the question of the degree of coherency should be addressed at an even lower level than we do here, since one should also consider how the various contributions to the on-site hyperfine fields are added together. For simplicity, however, we postpone this discussion to a future publication.

The essential asset of the model presented in this paper is that a same (fast) fluctuation mechanism of the spin liquid can be identified in the relaxation of all the nuclei (copper, oxygen, and yttrium), and this mechanism is characterized by a temperature-dependent effective correlation time $\tau_{eff}(T)$. Moreover, the parametrization $\tau_{eff}^{-1}=\tau_1^{-1}+\tau_2^{-1}$ has a wide range of validity. At low temperature, the effective correlation time τ_{eff} is just τ_1, which is linear in $YBa_2Cu_3O_7$ but is modified by a gap function in the underdoped compounds. In $YBa_2Cu_3O_7$, the term τ_1 could be linked to the nuclear relaxation by charge carriers in metals. At high temperature, the effective correlation time τ_{eff} goes over to the constant τ_2, which could be connected to the correlation time in antiferromagnets. This seems to indicate that at high temperature, the nuclei are probably influenced by a system of local moments not very different from the paramagnetic phase of the underdoped parent compounds. Lowering the temperature, a smooth crossover to an itinerant system is observed. It looks like these features, which have been observed by Imai *et al.*[42] in La_2CuO_4, are also present in the YBaCuO system, although the crossover happens at higher temperatures. At low temperature, even in the optimally doped $YBa_2Cu_3O_7$, a seemingly local pairing of moments occurs that is reflected in the Curie-Weiss behavior of $\chi'(\vec{Q})$. Further analysis, however, is required to get more quantitative results about the doping dependence of all these phenomena. It should be mentioned that heavy fermions and mixed-valence systems also exhibit a crossover from localized moments to coherent behavior with decreasing temperature, as has been pointed out.[45]

We also note that the incommensuration or discommensuration of the AFM ordering observed by neutron scattering measurements does not invalidate the model presented here.[50] Moreover, the model (26a) has a wide range of applications, extending also to electron-doped superconductors. In particular, the NMR measurements taken by Imai *et al.*[46] on $Sr_{0.9}La_{0.1}CuO_2$ can also be fitted within our model.

Another important conclusion is that having identified a similar basic nuclear relaxation rate for all nuclei, the different temperature behavior of the observed rate of the copper and oxygen can be ascribed to the particular values of the hyperfine field constants. A detailed discussion (Sec. IV F) of the functions ${}^kV_\alpha(T)$ showed the crucial interplay of nearest neighbors and higher AFM correlations and revealed the complications one meets in trying to find Korringa relations in layered cuprates. A case of practical interest is that the on-site and transferred hyperfine energies for Cu are such that ${}^{63}V_{ab}(T)$ (which determines ${}^{63}T_{1c}^{-1}$) changes only slightly, since the contributions from the nearest-neighbor and the next-next-nearest-neighbor correlations nearly cancel each other out.

We proposed in this paper an alternative way of looking at the spin-lattice relaxation data that we believe could help identify the underlying physical processes in the cuprates. The analysis of the selected set of data in cuprates shows that the present model reveals the wealth of information that can be obtained from NMR and NQR measurements. While the success of the parametrization $\tau_{eff}^{-1}(T)=\tau_1^{-1}(T)+\tau_2^{-1}$ is surprisingly good and universal, we could only suggest likely explanations about its significance, and a conclusive interpretation is still open to speculation.

ACKNOWLEDGMENTS

We would like to thank A. Höchner, who determined in the framework of his diploma thesis the hyperfine field constants used as starting values in this work. We are particularly grateful to M. Mali and J. Roos for providing much insight in the experimental work and for many fruitful discussions. We also appreciate interesting discussions with D. Brinkmann, H. R. Ott, and T. M. Rice. We thank also our colleagues E. Stoll and S. Renold for their valuable input. P.F.M. thanks C. P. Slichter for inspiring discussions. This work was supported by the Swiss National Science Foundation.

APPENDIX A: SCALED CONTRIBUTIONS TO THE RELAXATION RATES

The quantities ${}^kU_\alpha$ extracted from the experiments can be gathered into one plot, each on a different scale. This is equivalent to applying the affine transformation

$$ {}^k\bar{U}_\alpha = {}^kf_\alpha\,{}^kU_\alpha + {}^kg_\alpha, \tag{A1}$$

with constants ${}^kf_\alpha$ and ${}^kg_\alpha$. The result for $YBa_2Cu_3O_7$ is shown in Fig. 22(a), where the vertical axis is arbitrary.We note that the ${}^kU_\alpha$ in $YBa_2Cu_3O_7$ have the same temperature dependence for most of the temperature range. The larger deviations occur at higher temperature for ${}^{63}U_{ab}$ (thick dashed-dotted line) and ${}^{17}U_b$ (thin dotted line). The same operations can be done for $YBa_2Cu_3O_{6.63}$ [Fig. 22(b)].

Again, all ${}^{k}U_{\alpha}$ fall on the same curve, apart from ${}^{63}U_{ab}$, which deviates significantly.

A similar picture is drawn upon dividing the rates ${}^{k}U_{\alpha}(T)$ by the constants ${}^{k}V_{\alpha}^{0}$, which are calculated from (15) and whose values are gathered in Table II, ${}^{k}\tilde{U}_{\alpha}(T) := {}^{k}U_{\alpha}(T)/{}^{k}V_{\alpha}^{0}$. The scaled relaxation rates ${}^{k}\tilde{U}_{\alpha}(T)$ are shown in Fig. 23 for $YBa_2Cu_3O_7$ and $YBa_2Cu_3O_{6.63}$.

APPENDIX B: DETAILED INVESTIGATION OF ${}^{k}V_{\alpha}(T)$ AND KORRINGA-LIKE BEHAVIOR

We plotted in Fig. 24 the individual contributions to ${}^{63}V_{\alpha}(T)$, which are defined as

$$
\begin{aligned}
{}^{63}V_{\alpha}^{1}(T) &= \frac{1}{4\hbar^2}[8A_{\alpha}BK_{01}^{\alpha}(T)],\\
{}^{63}V_{\alpha}^{2}(T) &= \frac{1}{4\hbar^2}[8B^2K_{12}^{\alpha}(T)],\\
{}^{63}V_{\alpha}^{3}(T) &= \frac{1}{4\hbar^2}[4B^2K_{13}^{\alpha}(T)].
\end{aligned}
\tag{B1}
$$

${}^{63}V_{\alpha}^{1}$, ${}^{63}V_{\alpha}^{2}$, and ${}^{63}V_{\alpha}^{3}$ are the terms proportional, respectively, to the AFM spin correlation functions K_{01}^{α}, K_{12}^{α}, and K_{13}^{α}. We also have the constant term ${}^{63}V_{\alpha}^{0}$, the temperature-independent contribution given in Eq. (15a) and Table II. Since $A_{ab}>0$, $A_c<0$, $K_{01}^{\alpha}\leqslant 0$, and $K_{12}^{\alpha}, K_{13}^{\alpha}\geqslant 0$, all individual contributions ${}^{63}V_{\alpha}^{i}$ are positive except ${}^{63}V_{ab}^{1}$. We see in Fig. 24(a) that ${}^{63}V_{ab}$ (large circles) is made up almost entirely of ${}^{63}V_{ab}^{0}+{}^{63}V_{ab}^{2}$ (small circles), whereas ${}^{63}V_{c}$ in Fig. 24(b) (large triangles) is dominated by ${}^{63}V_{c}^{0}+{}^{63}V_{c}^{1}$ (small triangles). In other words, in the *ab* direction, ${}^{63}V_{ab}^{1}$ and ${}^{63}V_{ab}^{3}$, having opposite signs, almost cancel each other out. For example, near T_c, where the correlations are high, $|{}^{63}V_{ab}^{1}/{}^{63}V_{ab}^{3}| = 2A_{ab}/B|K_{01}^{ab}|/|K_{01}^{ab}|^2 \approx 1$. In the *c* direction, all contributions have the same sign, but due to the high value of $|A_c|$, the lower-order correlation plays the major role. Note that the same qualitative behavior is expected, irrespective of the choice of correlation dependence [Eq. (17)].

The seemingly Korringa-like behavior of $({}^{17}T_{1\alpha}T)^{-1}$ is investigated in Fig. 25. There we decomposed ${}^{17}T_{1c}^{-1} \propto (1-|K_{01}^{ab}|)\tau_{eff}$ (solid line) into

$$
(1-|K_{01}^{ab}|)\tau_{eff} = \tau_1 + (\tau_{eff}-\tau_1) - \tau_{eff}|K_{01}^{ab}|. \tag{B2}
$$

From Fig. 25, we see that the contribution $\tau_{eff}|K_{01}^{ab}|$ (dotted line) varies little over a large range of temperature. The dashed line is the truly linear contribution τ_1. The actual temperature dependence of $({}^{17}T_{1\alpha}T)^{-1}$ is thus given by this linear contribution, minus that of $(\tau_{eff}-\tau_1)$ (dashed-dotted line). The total result has, however, the appearance of linearity.

[1] D. Brinkmann and M. Mali, *NMR Basic Principles and Progress* (Springer, Heidelberg, 1994), Vol. 31.

[2] C. P. Slichter, in *Strongly Correlated Electronic Materials, The Los Alamos Symposium*, edited by K. S. Bedell, Z. Wang, D. Meltzer, A. V. Balatsky, and E. Abrahams (Addison-Wesley, Reading, MA, 1993), p. 427.

[3] C. Berthier, M. H. Julien, M. Horvatic, and Y. Berthier, J. Phys. I **6**, 2205 (1996).

[4] A. Rigamonti, F. Borsa, and P. Caretta, Rep. Prog. Phys. **61**, 1367 (1998).

[5] W. W. Warren, R. E. Walstedt, G. F. Brennert, G. P. Espinosa, and J. P. Remeika, Phys. Rev. Lett. **59**, 1860 (1987).

[6] T. Imai, T. Shimizu, T. Tsuda, H. Yasuoka, T. Takabatake, and Y. Nakazawa, J. Phys. Soc. Jpn. **57**, 1771 (1988).

[7] T. Imai, T. Shimizu, H. Yasuoka, Y. Ueda, and K. Kosuge, J. Phys. Soc. Jpn. **57**, 2280 (1988).

[8] P. C. Hammel, M. Takigawa, R. H. Heffner, Z. Fisk, and K. C. Ott, Phys. Rev. Lett. **63**, 1992 (1989).

[9] W. W. Warren, R. E. Walstedt, G. F. Brennert, R. J. Cava, R. Tycko, R. F. Bell, and G. Dabbagh, Phys. Rev. Lett. **62**, 1193 (1989).

[10] R. E. Walstedt, W. W. Warren, R. F. Bell, R. J. Cava, G. P. Espinosa, L. F. Schneemeyer, and J. V. Waszczak, Phys. Rev. B **41**, R9574 (1990).

[11] T. Imai, K. Yoshimura, T. Uemura, H. Yosuoka, and K. Kosuge, J. Phys. Soc. Jpn. **59**, 3846 (1990).

[12] M. Takigawa, A. P. Reyes, P. C. Hammel, J. D. Thompson, R. H. Heffner, Z. Fisk, and K. C. Ott, Phys. Rev. B **43**, 247 (1991).

[13] R. E. Walstedt, B. S. Shastry, and S. W. Cheong, Phys. Rev. Lett. **72**, 3610 (1994).

[14] F. Mila and T. M. Rice, Physica C **157**, 561 (1989).

[15] H. Monien, D. Pines, and C. P. Slichter, Phys. Rev. B **41**, 11120 (1990).

[16] A. J. Millis, H. Monien, and D. Pines, Phys. Rev. B **42**, 167 (1990).

[17] Y. Zha, V. Barzykin, and D. Pines, Phys. Rev. B **54**, 7561 (1996).

[18] C. P. Slichter, *Principles of Magnetic Resonance* (Springer, Berlin, 1996).

[19] C. H. Pennington, D. J. Durand, C. P. Slichter, J. P. Rice, E. D. Bukowski, and D. M. Ginsberg, Phys. Rev. B **39**, R2902 (1989).

[20] B. S. Shastry, Phys. Rev. Lett. **63**, 1288 (1989).

[21] P. Hüsser, H. U. Suter, E. P. Stoll, and P. F. Meier, Phys. Rev. B **61**, 1567 (2000).

[22] S. Renold, S. Plibersek, E. P. Stoll, T. A. Claxton, and P. F. Meier, Eur. Phys. J. B **23**, 3 (2001).

[23] A. Suter, M. Mali, J. Roos, D. Brinkmann, J. Karpinski, and E. Kaldis, Phys. Rev. B **56**, 5542 (1997).

[24] P. F. Meier, Physica C **364–365**, 411 (2001).

[25] R. E. Walstedt, W. W. Warren, R. F. Bell, G. F. Brennert, G. P. Espinosa, R. J. Cava, L. F. Schneemeyer, and J. V. Waszczak, Phys. Rev. B **38**, R9299 (1988).

[26] J. A. Martindale, P. C. Hammel, W. L. Hults, and J. L. Smith, Phys. Rev. B **57**, 11769 (1998).

[27] M. Takigawa, W. L. Hults, and J. L. Smith, Phys. Rev. Lett. **71**, 2650 (1993).

[28] A. Höchner, Diploma thesis, Zürich Universität, 2002.

[29] V. A. Nandor, J. A. Martindale, R. W. Groves, O. M. Vyaselev, C. H. Pennington, L. Hults, and J. L. Smith, Phys. Rev. B **60**, 6907 (1999).

[30] D. Pines and C. P. Slichter, Phys. Rev. **100**, 1014 (1955), which is known as the "Wabash Cannonball Paper" because it was written during the train ride to Detroit for the 1955 APS March meeting [C. P. Slichter (private communication)].

[31] S. E. Barrett, J. A. Martindale, D. J. Durand, C. H. Pennington, C. P. Slichter, T. A. Friedmann, J. P. Rice, and D. M. Ginsberg, Phys. Rev. Lett. **66**, 108 (1991).

[32] C. H. Pennington and C. P. Slichter, Phys. Rev. Lett. **66**, 381 (1991).

[33] T. Imai, C. P. Slichter, A. P. Paulikas, and B. Veal, Appl. Magn. Reson. **3**, 729 (1992).

[34] T. Imai, C. P. Slichter, A. P. Paulikas, and B. Veal, Phys. Rev. B **47**, R9158 (1993).

[35] J. Haase, D. K. Morr, and C. P. Slichter, Phys. Rev. B **59**, 7191 (1999).

[36] A. Uldry, M. Mali, J. Roos, and P. F. Meier, cond-mat/0506245 (unpublished).

[37] F. Raffa, T. Ohno, M. Mali, J. Roos, D. Brinkmann, K. Conder, and M. Eremin, Phys. Rev. Lett. **81**, 5912 (1998).

[38] N. J. Curro, T. Imai, C. P. Slichter, and B. Dabrowski, Phys. Rev. B **56**, 877 (1997).

[39] I. Tomeno, T. Machi, K. Tai, N. Koshizuka, S. Kambe, A. Hayashi, Y. Ueda, and H. Yasuoka, Phys. Rev. B **49**, 15327 (1994).

[40] J. Haase, C. P. Slichter, and C. T. Milling, J. Supercond. **15**, 339 (2002).

[41] S. Ohsugi, Y. Kitaoka, K. Ishida, G. Q. Zheng, and K. Asayama, J. Phys. Soc. Jpn. **63**, 700 (1994).

[42] T. Imai, C. P. Slichter, K. Yoshimura, and K. Kosuge, Phys. Rev. Lett. **70**, 1002 (1993).

[43] T. Moriya, Prog. Theor. Phys. **16**, 641 (1956).

[44] J. Haase, C. P. Slichter, R. Stern, C. T. Milling, and D. G. Hinks, J. Supercond. **13**, 723 (2000).

[45] N. J. Curro, B.-L. Young, J. Schmalian, and D. Pines, Phys. Rev. B **70**, 235117 (2004).

[46] T. Imai, C. P. Slichter, J. L. Cobb, and J. T. Markert, J. Phys. Chem. Solids **56**, 1921 (1995).

[47] D. R. Harshman and A. P. Mills, Phys. Rev. B **45**, 10684 (1992).

[48] One can identify three contributions to the components of the general hyperfine interaction tensor, the isotropic (Fermi contact) term, the traceless dipolar term, and the spin-orbit coupling term. We note that the core polarization is not an observable. We use instead the total Fermi contact interaction, which can consist of on-site as well as transferred contributions. The mechanisms of spin transfer and the radial dependence of the difference between spin-up and spin-down densities at the oxygen and the copper have been illustrated by cluster calculations (see Ref. 22).

[49] In comparison, Harshman and Mills (Ref. 47) found $T_F = 2290 \pm 100$ K.

[50] We recall that the essential quantity in the present approach is the nearest-neighbor spin correlation K_{01}^{α}, which, for $YBa_2Cu_3O_7$, changes from -0.4 at $T=100$ K to -0.2 at room temperature. Whether these values are due to incommensurability or discommensurability accompanied with fast fluctuations does not matter. Differences will occur in the correlations K_{12}^{α} and K_{13}^{α}. A detailed investigation will be published elsewhere.